CIRCUIT MODELLING
OF
POWER BIPOLAR JUNCTION TRANSISTOR

by
Sqn Ldr VIPUL VIJ

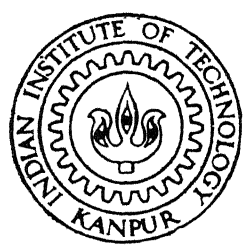

DEPARTMENT OF ELECTRICAL ENGINEERING
INDIAN INSTITUTE OF TECHNOLOGY KANPUR

MARCH, 1998

CIRCUIT MODELLING
OF
POWER BIPOLAR JUNCTION TRANSISTOR

A Thesis Submitted
in Partial Fulfilment of the Requirements
for the Degree of
MASTER OF TECHNOLOGY

by

Sqn Ldr VIPUL VIJ

to the

Department of Electrical Engineering
Indian Institute of Technology, Kanpur

March 1998.

CERTIFICATE

This is to certify that the present M.Tech Thesis work titled **Circuit Modelling of Power Bipolar Junction Transistor**, *has been carried out by* **Sqn Ldr Vipul Vij** *under my supervision and it has not been submitted elsewhere for a degree.*

March 98

Dr. M. B. Patil
Assistant Professor
Department of Electrical Engineering
Indian Institute of Technology
Kanpur

Abstract

A Power Bipolar Junction Transistor (PBJT) model is developed giving both static and dynamic behavior. The ordinary differential equations are derived based on the semiconductor physics. These equations take into account the recombination, charging and discharging process in the lightly doped collector drift region. The model is implemented along with associated circuitry, like base drive, load (resistive and inductive), by writing a $C-$ program. The static behavior giving quasi-saturation characteristics can be simulated with this model. The transient behavior of the model is studied with different base drives, time steps and error margins. Also charge profile in the drift region is presented at different instants during turn on/off. Experimental results , wherever available, are plotted along with simulated results. The matching between the two validates the model developed. Also qualitative agreement with published work exists for various simulated results presented in this thesis work.

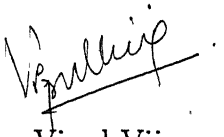

Vipul Vij

Sqn Ldr

ACKNOWLEDGEMENT

I am deeply indebted to **Dr. M. B. Patil**, for his inspiring guidance and encouragement at every stage of this thesis. He provided me with numerous constructive suggestions, without which this work would not have been possible. I am also grateful to him for the patience displayed during those numerous discussions.

Above all I am also thankful to Lord "*Sai*" for giving me wisdom, courage and sufficient knowledge for undertaking and completing this work successfully.

Vipul Vij

Sqn Ldr

Contents

List of Figures

List of Tables

Chapter 1

INTRODUCTION

The Power Bipolar Junction Transistor (PBJT) differs in many respects in contrast to the low-voltage BJT. In PBJT there is a need for large blocking voltage in the off-state and a high current carrying capability in the on-state. This leads to a difference in structure and doping profile of a PBJT. Due to different structure and doping profile the I V characteristics and switching behavior of a PBJT is quite different from a low-voltage BJT. Due to above mentioned reasons low-voltage BJT models are not suitable or applicable for the PBJTs. In this work a PBJT model is developed which gives both static and dynamic behavior under different bias conditions. This model is derived and implemented from the study of various works published in this field as given in references [1]-[4].

1.1 Structure of PBJT

There are many structures of PBJT e.g. $n^+p\,n^+$, $n^+p\,\nu\,n^+$, $n^+p\,\nu\,n\,n^+$ etc. The PBJT structure considered for modelling in this work is $n^+p\,\nu\,n^+$ structure. The structure of the PBJT is shown in Fig. 1.1.

The PBJT has a vertically oriented four layer structure . The vertical structure is preferred for power transistors because it maximizes the cross-sectional area

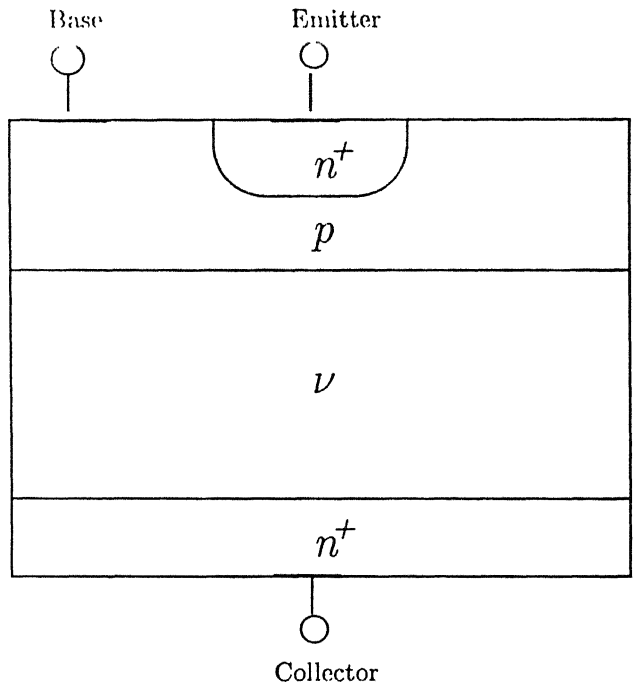

Figure 1.1: Structure of PBJT

through which the current in the device is flowing. This minimizes the on-state resistance and thus the power dissipation in the transistor.

The doping levels in each of the layers and the thickness of the layers have a significant effect on the characteristics of the device. The doping in the emitter layer is quite large (typically 10^{19} cm^{-3}), whereas base doping is moderate (10^{16} cm^{-3}). The ν-region called the drift region has a light doping level (10^{14} cm^{-3}). The n^+ region that terminates the drift region has a doping level similar to that found in the emitter. The thickness of the drift region determines the breakdown voltage of the transistor and thus can range from tens to hundreds of microns in extent.

Practical power transistors have their emitter and bases interleaved as narrow fingers to reduce the effect of current crowding, a phenomenon that can lead to device failure. This type of structure also reduces the parasitic ohmic resistance in the base current path, which helps to reduce power dissipation in the transistor.

1.2 Basic Model of PBJT

The PBJT characteristics are dominated by the charge in the lightly doped collector layer (drift region) which is negligible or non-existent in a low-voltage BJT. This must be considered and described in a generic PBJT model. The basic model is as shown in the Fig. 1.2 [5].

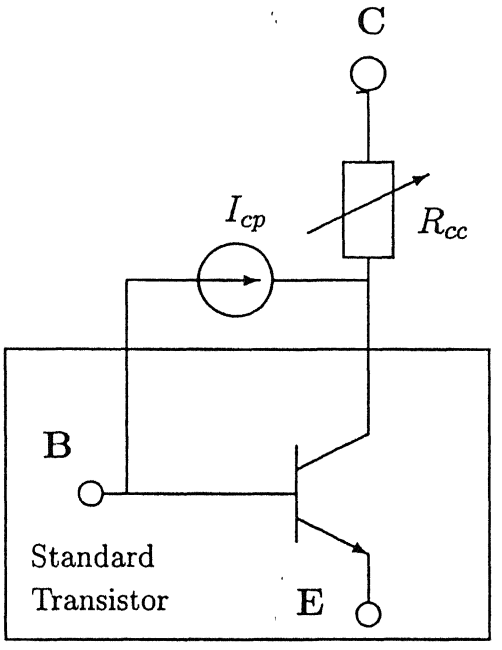

Figure 1.2: PBJT Model

The model consists of a standard BJT model and two additional elements, the collector resistance R_{cc} and a current source I_{cp}. R_{cc} is added to take care of the voltage drop in the drift region and I_{cp} basically describes the recombination taking place in collector layer. I_{cp} is hole current from base into the collector. The recombination in collector layer is not negligible in spite of high lifetime and thus must be incorporated in the model. These two elements along with standard BJT model are able to describe both static and dynamic characteristics of PBJT.

1.3 Basic Approach for Computer Simulation

A widely accepted approach to the fundamental modelling of semiconductor devices involves the solution of the semiconductor device equations, which comprise Poisson's equation and the hole and electron continuity equation. This, however, is often impractical as it takes a large CPU time and memory. In this work, we treat the PBJT with a circuit model instead, and solve the circuit equations together with the model equations. The Newton-Raphson iteration method is used to solve the set of nonlinear differential equations. A second order integration method is used for implicit time stepping i.e. Gear-Shichman integration method. The convergence to a solution is controlled by keeping a very low error margin of about 10^{-6}. The basic algorithm flow chart is given in Fig. 1.3.

First the circuit to be simulated, i.e., PBJT and the external elements like supply voltages, load, etc. are converted into a set of equations in the form of matrices. The DC analysis of the circuit is carried out to find the bias point. The matrices are solved using gaussian elimination method. For transient analysis the results of DC analysis supply an initial guess. All the derivatives are removed using Gear-Shichman integration method. Time step is set to be about one hundredth of minority carrier lifetime. The equations are then solved at each time step using Newton-Raphson iterations and error is worked out. Convergence is only achieved if error goes below 10^{-6} at each node. The results thus achieved supply guess for next time step.

The results thus achieved are checked and compared with the published results. Quite good agreement is achieved in this.

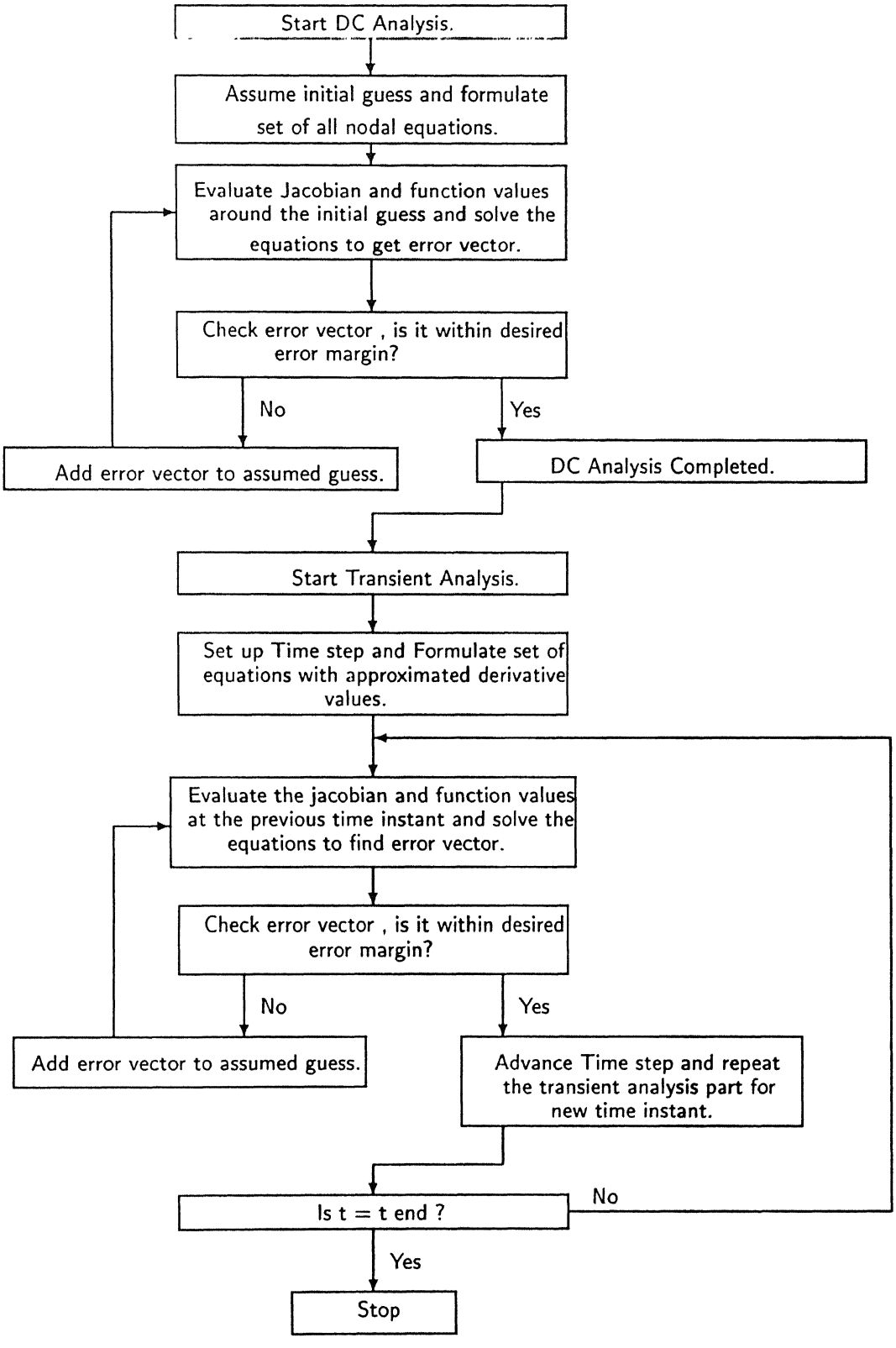

Figure 1.3: Flow Chart for PBJT Simulation (Static and Dynamic)

Chapter 2

MODEL DESCRIPTION

2.1 The Static Model

The basic equations governing the transport of carriers are the Poisson, the current density, and the continuity equations. As the collector layer is at least partially high injection in the on state ($n \approx p$), the following equations describe the minority carrier distribution $p(x)$ in the high injection region for a one dimensional current transport, which is assumed for the collector layer [5].

$$j_p = \frac{1}{b+1} j - e D \frac{\partial p}{\partial x} \tag{2.1}$$

$$\frac{1}{e} \frac{\partial j_p}{\partial x} = -\Re - \frac{\partial p}{\partial t} = -\frac{p}{\tau} - \frac{\partial p}{\partial t} \tag{2.2}$$

where e is the electron charge, b the ratio between electron and hole mobility, and D the ambipolar diffusion constant, j and j_p are the total current and hole current density, respectively, $\Re$ is the recombination rate. A constant lifetime τ is assumed.

At steady state ($\partial/\partial t = 0$), eqns. (2.1) and (2.2) are reduced to an ordinary differential equation, given by

$$\frac{d^2 p}{dx^2} = \frac{p}{D\tau} = \frac{p}{L^2} \tag{2.3}$$

where L is the ambipolar diffusion length. This is a second order differential equation. The solution of this equation is a hyperbolic function.

$$p(x) = C_1 \cosh \frac{x}{L} + C_2 \sinh \frac{x}{L} \tag{2.4}$$

where C_1 and C_2 are constants which can be found using boundary conditions [5]. Figure 2.1 gives the charge profile in the drift region of PBJT. The boundary

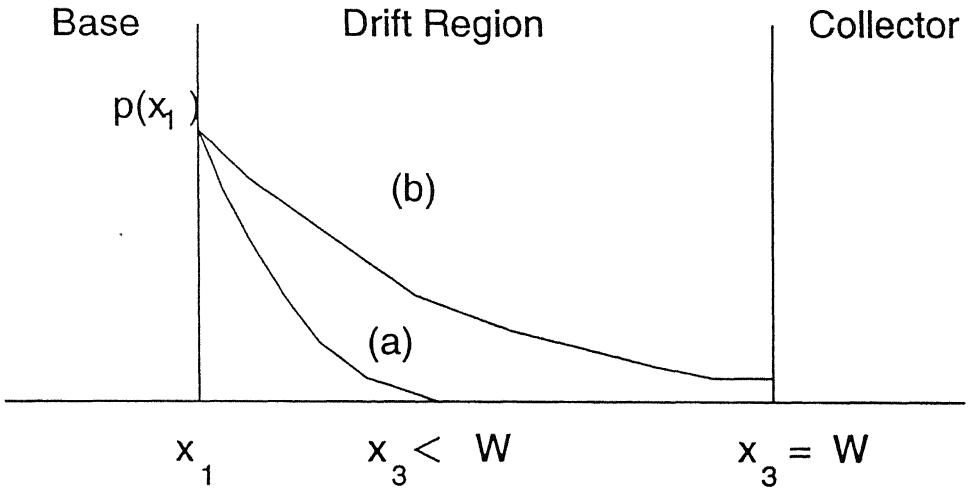

Figure 2.1: Charge Profile in Drift Region of PBJT (a) Quasi-Saturation (b) Hard-Saturation

conditions are given by the following equations.

$$p(x_1) = n_i \exp\left(\frac{V_{bc}}{2\,V_T}\right) \tag{2.5}$$

$$\left|\frac{\partial p}{\partial x}\right|_{x=x_1} = -\frac{i_c + (b+1)\,I_{cp}}{e\,(b+1)\,D\,A} \tag{2.6}$$

$$\left|\frac{\partial p}{\partial x}\right|_{x=x_3} = -\frac{i_c}{e\,(b+1)\,D\,A} \tag{2.7}$$

where $p(x_1)$ is the carrier concentration at the base-collector boundary, n_i is the intrinsic carrier density, V_T is the thermal voltage, and V_{bc} is the internal base-collector voltage, i.e., between the base and collector of the standard transistor of

Fig. 1.2. x_1 and x_3 are the edges of the injected charge towards the base and the n^+ collector contact, respectively as depicted in Fig. 2.1. i_c is the collector current, I_{cp} is the recombination current and A is the collector base junction area.

If the charge distribution is such that after turn-on x_3 is not able cover the entire width of the collector drift region then the transistor is operating in the quasi-saturation region; else in the hard-saturation region as depicted in Fig. 2.1.

Thus there are two possible solutions for the collector layer. Now if W is the width of the collector drift region then the solution for quasi-saturation are as given below.

From eqns. (2.4) and (2.5)

$$C_1 = p(x_1) \tag{2.8}$$

where $x = x_1 = 0$

Also for Quasi-saturation $p(x_3) = 0$. Thus from eqn. (2.4)

$$C_2 = -\frac{p(x_1)\cosh\frac{x_3}{L}}{\sinh\frac{x_3}{L}} \tag{2.9}$$

Substituting C_1 and C_2 in eqn. (2.4) , we get

$$p(x) = p(x_1)\frac{\sinh\frac{x_3-x}{L}}{\sinh\frac{x_3}{L}} \tag{2.10}$$

Applying boundary condition of eqn. (2.7) on eqn. (2.10), we get

$$x_3 = L\sinh^{-1}\left[\frac{e\,(b+1)\,D\,A\,p(x_1)}{i_c\,L}\right] < W \tag{2.11}$$

Applying boundary condition given by eqn. (2.6) on eqn. (2.10), we get

$$I_{cp} = \frac{e\,D\,A\,p(x_1)}{L}\,\frac{\cosh\left(\frac{x_3}{L}\right)-1}{\sinh\frac{x_3}{L}} \tag{2.12}$$

R_{cc} consists of two parts, i.e., resistance of the charge induced part(R_{c1}) and resistance of the unmodulated part(R_{c2}) of drift region. Now R_{c1} and R_{c2} can be calculated by calculating the voltage drop in the respective drift region parts(V_{c1}, V_{c2}).

If the drop due to the recombination current I_{cp} is neglected then R_{c1}, R_{c2} can be calculated in the following manner [9],

$$R_{c1} = \frac{V_{c1}}{i_c} = V_T \ln\left(1 + \frac{p(x_1)}{N_D}\right)$$

$$R_{c2} = \frac{V_{c2}}{i_c} = R_{co}\left(1 - \frac{x_3}{W}\right)$$

Where R_{co} is the resistance of drift region without injection of any charge and N_D is the doping density of the drift region. R_{cc} is given by the following relation.

$$R_{cc} = R_{c1} + R_{c2}$$

substituting values of R_{c1}, R_{c2}, we get the following relation for R_{cc}.

$$R_{cc} = R_{co}\left(1 - \frac{x_3}{W}\right) + \frac{V_T}{i_c} \ln\left(1 + \frac{p(x_1)}{N_D}\right) \tag{2.13}$$

and the solutions for hard-saturation are

$$x_3 = W \tag{2.14}$$

C_1 and C_2 can again be evaluated using eqns. (2.5) and (2.4). C_1 is same as in eqn. (2.8) and C_2 is as follows.

$$C_2 = \frac{p(x_3) - p(x_1)\cosh\frac{W}{L}}{\sinh\frac{W}{L}} \tag{2.15}$$

$p(x_3)$ can be evaluated using boundary condition given by eqn. (2.7) and the value thus obtained can be used to evaluate C_2. Substituting C_1 and C_2 in eqn. (2.4) , we get

$$p(x) = \frac{p(x_1)\cosh\frac{W-x}{L} - \frac{i_c L}{e(b+1)DA}\sinh\frac{x}{L}}{\cosh\frac{W}{L}} \tag{2.16}$$

Applying boundary condition given by eqn. (2.6) on eqn. (2.16) , we get

$$I_{cp} = \frac{e\,D\,A\,p(x_1)}{L}\tanh\frac{W}{L} - \frac{i_c}{b+1}\frac{\cosh\left(\frac{W}{L}\right) - 1}{\cosh\frac{W}{L}} \tag{2.17}$$

$$R_{cc} = \frac{V_T}{I_c} \ln \left(\frac{p(x_1) + N_D}{p(x_3) + N_D} \right) \tag{2.18}$$

Again R_{cc} is calculated in the similar way as in the quasi-saturation case, only difference being that, now entire drift region is charge injected so there is only one type of voltage drop which can be calculated knowing $p(x_1)$, $p(x_3)$ as given in [9]. In calculation of R_{cc} voltage drop due to recombination is neglected as it is very small as compared to other voltage drops in the PBJT.

The circuit model for modelling the static characteristics of PBJT is given in Fig. 2.2. The equivalent circuit of PBJT model of Fig. 2.2 is given in Fig. 2.3. The standard transistor of basic model is represented by the Ebers-Molls equivalent circuit.

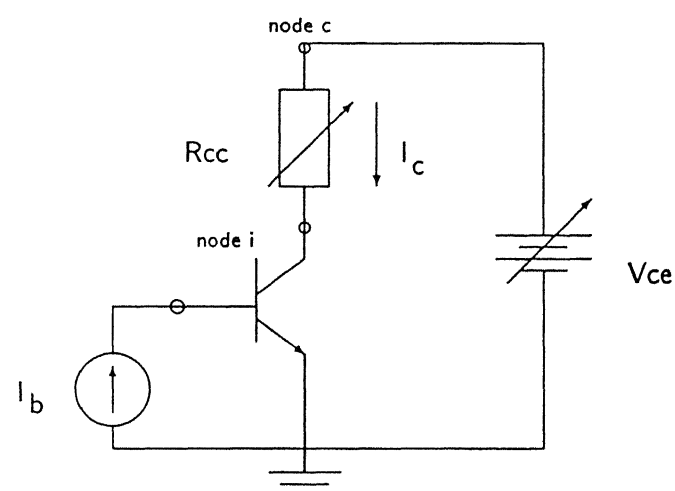

Figure 2.2: PBJT Circuit (Static Case)

A constant current source I_b is assumed. From the figure it is clear that there are three nodes (b, i, c). The node b is the base node, node i is the internal collector node, i.e., collector node of standard transistor, and node c is the collector node of PBJT. V_{ce} is variable voltage source. For nodes b and i, KCL is written and Branch Constitutive Equation (BCE) is written for node c.

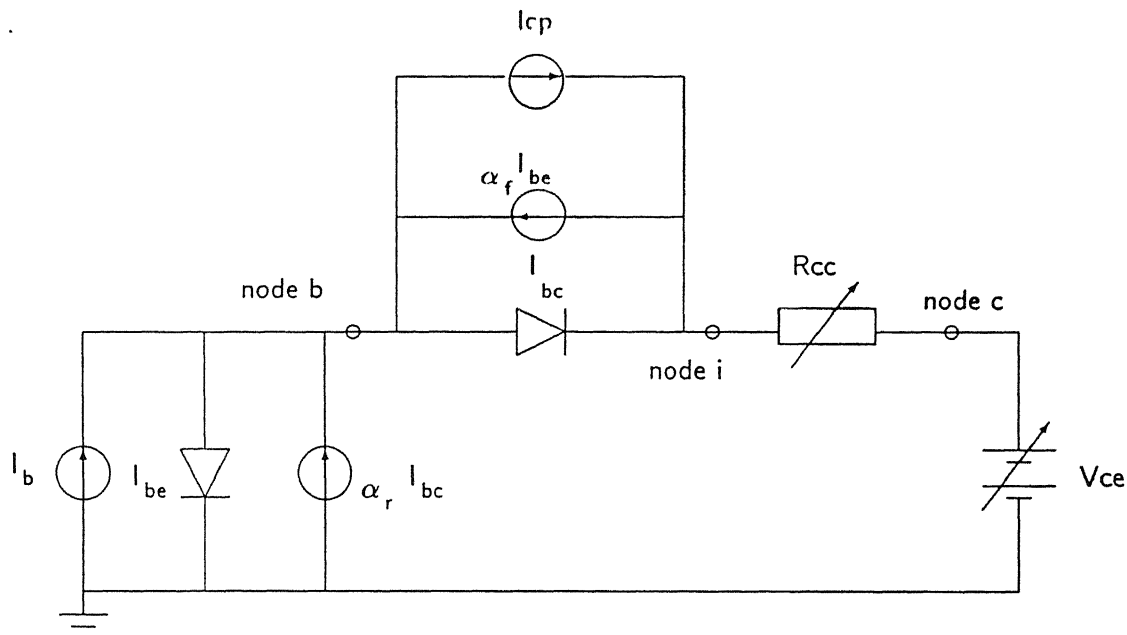

Figure 2.3: PBJT Equivalent Circuit (Static Case)

$$f_1(v_b, v_i, i_c) \equiv I_{be}(1-\alpha_f) + I_{bc}(1-\alpha_r) + I_{cp} - I_b = 0 \tag{2.19}$$

$$f_2(v_b, v_i, i_c) \equiv -I_{cp} - I_{bc} + \alpha_f I_{be} - i_c = 0 \tag{2.20}$$

$$f_3(v_b, v_i, i_c) \equiv V_{ce} - v_i - i_c R_{cc} = 0 \tag{2.21}$$

where I_{cp} , R_{cc} are given by equations (2.12) or (2.17), and (2.13) or (2.18) respectively as the case may be and I_{be} and I_{bc} are as given below.

$$I_{be} = I_s \left[\exp\left(\frac{v_b}{v_t}\right) - 1\right] \tag{2.22}$$

$$I_{bc} = I_s \left[\exp\left(\frac{v_b - v_i}{v_t}\right) - 1\right] \tag{2.23}$$

where I_s is the reverse saturation current and f_1, f_2, f_3 are the functions of three unknowns.

The unknowns for the circuit simulation are node voltages at node b and i and node current through nodes c and i i.e. i_c, the collector current. An initial guess is assumed for the unknowns and equations are solved using Newton Raphson iteration technique as given below.

The function values and the partial derivatives of each function with respect to the unknowns are evaluated to form the following equations in matrices form.

$$\begin{bmatrix} \frac{\partial f_1}{\partial v_b} & \frac{\partial f_1}{\partial v_i} & \frac{\partial f_1}{\partial i_c} \\ \frac{\partial f_2}{\partial v_b} & \frac{\partial f_2}{\partial v_i} & \frac{\partial f_2}{\partial i_c} \\ \frac{\partial f_3}{\partial v_b} & \frac{\partial f_3}{\partial v_i} & \frac{\partial f_3}{\partial i_c} \end{bmatrix} \begin{bmatrix} \Delta v_b \\ \Delta v_i \\ \Delta i_c \end{bmatrix} = - \begin{bmatrix} f_1(v_b^0, v_i^0, i_c^0) \\ f_2(v_b^0, v_i^0, i_c^0) \\ f_3(v_b^0, v_i^0, i_c^0) \end{bmatrix} \tag{2.24}$$

where v_b^0, v_i^0, i_c^0 are the assumed values of v_b, v_i, i_c , first matrix is called the Jacobian and the column vector on left is the error vector. Equation (2.24) is solved using Gaussian elimination technique and value of the errors are worked out. If error for all the three unknowns is within desired error margin then the process stops else a new guess is generated by adding the error for each unknown into the previously assumed value. The iteration process continues till error matrix is reduced to within limits of desired error margin. This technique of solving non linear equations is known as Newton-Raphson Method. V_{ce} is varied to get the IV curve for a particular value of base current I_b . This process is applied for each new value of V_{ce} and the initial guess for each case is the solution at previous V_{ce} value.

2.2 The Dynamic Model

The circuit in Fig. 2.2 describes also the dynamic behavior, but some variation must be considered. The formulation of R_{cc} remains approximately valid. I_{cp} now

contains the variation of the charge in the collector layer.

$$I_{cp} = \frac{Q}{\tau} + \frac{dQ}{dt} \tag{2.25}$$

where Q is the stored charge in the lightly doped collector layer given by

$$Q = e\,A \int_{x_1}^{x_3} p(x)\,dx \tag{2.26}$$

To describe $p(x)$, eqns. (2.1) and (2.2) are reduced to a single equation.

$$\frac{\partial^2 p}{\partial x^2} = \frac{1}{D\,\tau}\left(p + \tau\,\frac{\partial p}{\partial t}\right) \tag{2.27}$$

The above equation must be reduced to an ordinary differential equation to get a network model. The approximation made to realize this model is [5]:

$$\frac{\partial p}{\partial t} = \frac{p}{T} \tag{2.28}$$

where T is a function of time but not of position. Thus eqn. (2.27) can be written as given below. This approximation is made for the simplicity of the model. Comment will be made on this approximation in chapter 4.

$$\frac{\partial^2 p}{\partial x^2} = \frac{1 + \frac{\tau}{T}}{D\,\tau}\,p = \pm\frac{1}{\lambda^2}\,p \tag{2.29}$$

where λ is the newly introduced effective ambipolar diffusion length. All the boundary conditions given by eqns. (2.5), (2.6) and (2.7) remain valid. Equation (2.29) can now be solved analytically.

In the static case,

$$\frac{dQ}{dt} = 0 \Rightarrow \frac{dp}{dt} = 0 \Rightarrow \frac{\tau}{T} = 0 \tag{2.30}$$

λ is identical with L. The solution for $p(x)$ is same as given by equations (2.10) or (2.16) as the case may be.

For turning on of PBJT:

$$\frac{dQ}{dt} > 0 \Rightarrow \frac{dp}{dt} > 0 \Rightarrow \frac{\tau}{T} > 0 \tag{2.31}$$

λ is smaller than L, now $p(x)$ will be a hyperbolic function as in the static case where λ will replace L, i.e, eqns (2.10) to (2.18) will have L replaced by λ.

For turning off of PBJT ($dQ/dt < 0$) there are three different cases:

(a) Charges are still injected into the collector layer ($I_{cp} > 0$).

$$\frac{dQ}{dt} > -\frac{Q}{\tau} \Rightarrow \frac{dp}{dt} > -\frac{p}{\tau} \Rightarrow \frac{\tau}{T} > -1 \tag{2.32}$$

λ is now greater than L and $p(x)$ is still a hyperbolic function where λ replaces L as for turn on.

(b) No charge is injected into or extracted from collector layer ($I_{cp} = 0$).

$$\frac{dQ}{dt} = -\frac{Q}{\tau} \Rightarrow \frac{dp}{dt} = -\frac{p}{\tau} \Rightarrow \frac{\tau}{T} = -1 \tag{2.33}$$

$p(x)$ is now a straight line given by

$$p(x) = p(x_1) - \frac{i_c}{e\,(b+1)\,D\,A}\,(x - x_1) \tag{2.34}$$

(c) Charge is removed from collector layer ($I_{cp} < 0$).

$$\frac{dQ}{dt} < -\frac{Q}{\tau} \Rightarrow \frac{dp}{dt} < -\frac{p}{\tau} \Rightarrow \frac{\tau}{T} < -1 \tag{2.35}$$

Now the sign of eqn. (2.29) is negative and $p(x)$ is a sinusoidal function given by

$$p(x,t) = C_1 \cos\left(\frac{x}{\lambda} + C_2\right) \tag{2.36}$$

again C_1, C_2 can be determined by applying boundary conditions mentioned before. Also I_{cp} can be evaluated in similar manner. Finally solution is:

$$p(x,t) = \frac{p(x_1)}{\sin\left(\frac{x_3}{\lambda}\right)} \cos\left[\frac{x - \left(x_3 - \frac{\pi}{2}\lambda\right)}{\lambda}\right] \tag{2.37}$$

$$I_{cp} = -\frac{i_c}{b+1}\left(1 - \cos\frac{x_3}{\lambda}\right) \tag{2.38}$$

where

$$x_3 = \lambda \sin^{-1}\left[\frac{p(x_1)\, e\,(b+1)\, D\, A}{\lambda\, i_c}\right] \tag{2.39}$$

Equation (2.28) is an approximation and is assumed only for a certain region. The model would be exact if the whole collector layer is divided in many such regions, but this approach will be very CPU time consuming. Therefore number of divided regions must be low to reduce the complexity of the model, i.e., the number of regions (each with its own time constant) should be as few as possible. Usually one time constant for the whole high injected region is sufficient. During turn off the reverse base current is sometimes very high so that $[i_c + (b+1)I_{cp}] < 0$. This means $\partial p/\partial x$ at $x = x_1$ is positive , the sign of slope of $p(x)$ changes in the high injection region, and $p(x)$ has a cusp [3]. This drive is called a strong drive. Here only one T (sinusoidal function) for $p(x)$ would violate the balance of electron and hole current and characterize the process of discharging inaccurately. In this case, two sinusoidal functions (regions) are necessary to describe the charge distribution from the cusp towards the base and the n^+ collector contact.

$$p(x,t) = \begin{cases} p_2 \cos\frac{x_2 - x}{\lambda_1} & \text{for } x_1 \le x \le x_2 \\ p_2 \cos\frac{x - x_2}{\lambda_2} & \text{for } x_2 \le x \le x_3. \end{cases} \tag{2.40}$$

where p_2 is the minority carrier concentration at the cusp and x_2 is the distance of the cusp from base collector junction. Also I_{cp} is evaluated in similar manner as described previously.

$$p_2 = \frac{i_c\, \lambda_2}{e\,(b+1)\, D\, A} \tag{2.41}$$

$$I_{cp} = -\frac{i_c}{b+1}\left[1 - \left(\frac{\lambda_2}{\lambda_1}\right)\right] \tag{2.42}$$

The value of λ can be worked out by the solution of eqn. (2.25) which is given by

$$Q = \tau\, I_{cp}\left(1 - e^{-t/\tau}\right) + Q_0\, e^{-t/\tau}\,. \tag{2.43}$$

where Q_0 is the charge in the drift region at $t = 0$. Now the value of Q can be worked out using eqn. (2.26). By substituting this value of Q in eqn. (2.43) and solving for λ, we get

$$\lambda = L^2 \left(1 - e^{-t/\tau}\right) + \frac{Q_0 D e^{-t/\tau}}{I_{cp}} \tag{2.44}$$

For turning on $Q_0 = 0$ and for turning off $Q_0 = \tau I_{cp0}$. Here I_{cp0} is the value of I_{cp} obtained after turn on is complete. Also if there are two time constants, we get the following relation.

$$\lambda_1 \lambda_2 = L^2 \left(1 - e^{-t/\tau}\right) + \frac{Q_0 D e^{-t/\tau}}{I_{cp}} \tag{2.45}$$

Also by the condition at the cusp [3].

$$I_n = b I_p \tag{2.46}$$

$$I_n = i_c + I_{cp} - \frac{\Delta Q_1}{\Delta t} \tag{2.47}$$

$$I_p = -\frac{\Delta Q_2}{\Delta t} \tag{2.48}$$

where I_n is the electron current, I_p is the hole current, Q_1 and Q_2 are the charges on both the sides of cusp. The above equation set yields the value of λ_1, λ_1. Thus all variables for transient analysis are known.

The circuit model for transient simulations for PBJT takes into account a base drive supply voltage and also a load at the output node, which can be resistive or inductive as the case may be. Also a snubber capacitor is added between the collector and emitter of PBJT to fasten the switch off time. In practical circuit usually a diode is used instead of a capacitor. The circuit model is illustrated in Fig. 2.4. The base drive voltage is positive during turn on and polarity changes instantly during the turn off.

To drive the equivalent circuit of Fig. 2.4, each diode of Fig. 2.3 is modelled as shown in Fig. 2.5 [6].

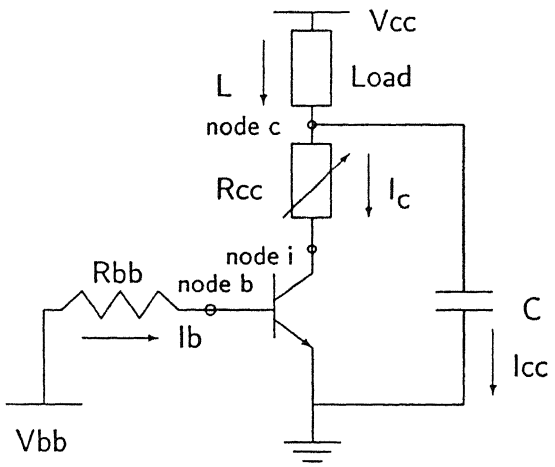

Figure 2.4: PBJT Circuit (Dynamic Case)

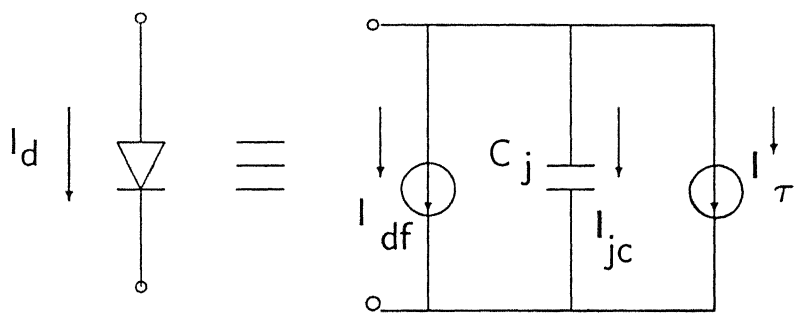

Figure 2.5: Diode Equivalent Circuit

where

$$I_d = I_{df} + I_{jc} + I_\tau \tag{2.49}$$

i.e., the total current flowing through diode constitutes of three subcomponents which can be modelled as

(a) DC current component I_{df} given by

$$I_{df} = I_s \left(\exp \frac{v_j}{V_T} - 1\right) \tag{2.50}$$

(b) Junction capacitance current component I_{jc}, given by

$$I_{jc} = \frac{dQ_{jc}}{dt} \tag{2.51}$$

where Q_{jc} is the charge associated with the junction capacitance C_{jc} given by

$$C_{jc} = \frac{C_{jo}}{\left(1 - \frac{v_j}{v_{bi}}\right)^{\frac{1}{2}}} \tag{2.52}$$

$$Q_{jc} = -2\, C_{jo}\, v_{bi} \left(1 - \frac{v_j}{v_{bi}}\right)^{\frac{1}{2}} \tag{2.53}$$

Here C_{jo} and v_{bi} are zero bias junction capacitance and built in junction potential respectively. Also v_j is the applied potential.

(c) Diffusion current component I_τ, given by

$$I_\tau = \tau \frac{dI_{df}}{dt} \tag{2.54}$$

Thus both the diodes of Fig. 2.3 can be expanded to generate equivalent circuit of Fig. 2.4. The equivalent circuit is given in Fig. 2.6.

The procedure for carrying out transient analysis again consists of writing the nodal equations and then solving them. Clearly there are three nodes as indicated in Fig. 2.6. For each node KCL and BCE are written. As we are concerned with the the transient analysis the equations will contain (d/dt) terms as well. These terms are approximated using Gear-Shichman approximation technique and then equations are solved in a similar manner as in the DC analysis case. However the choice of time-step is very important because a bigger time step can result in loss of transient behavior and a very small time step can result in too much of computation time. Usually time step is fixed at one hundredth of the minority carrier lifetime. The following set of equations illustrates the full procedure. Two cases are being considered, one for resistive load and other for inductive load.

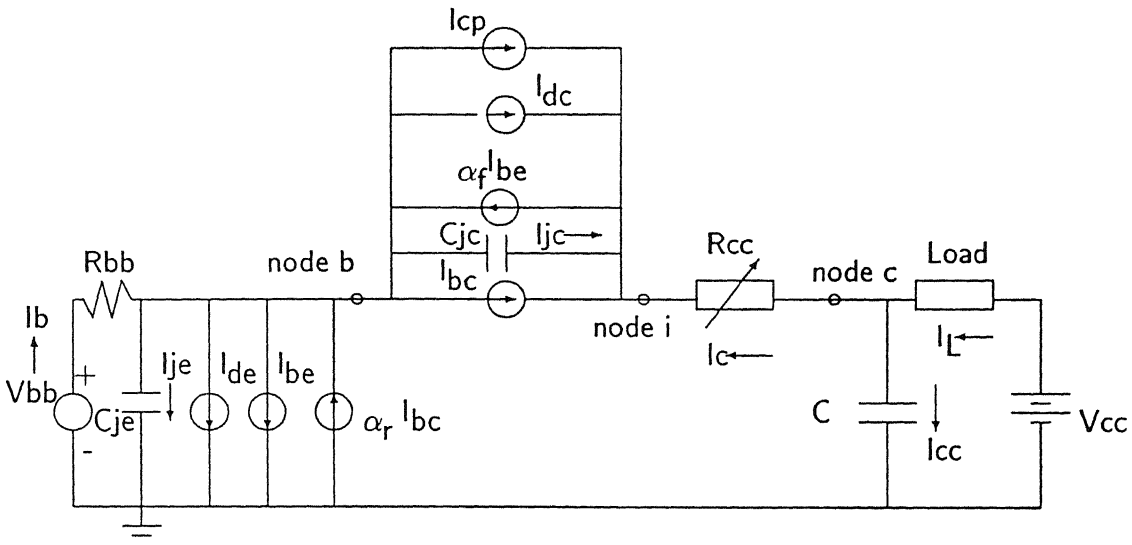

Figure 2.6: PBJT Equivalent Circuit (Dynamic Case)

2.2.1 Resistive Load

Writing KCL and BCE for each node.

Node b :

$$f_1 \equiv I_{be} + I_{je} + I_{de} - \alpha_r I_{bc} - I_b + I_{bc} + I_{cp} + I_{jc} + I_{dc} - \alpha_f I_{be} = 0 \qquad (2.55)$$

where I_{be}, I_{bc} are the dc current components, I_{je}, I_{jc} are the junction capacitance current components, and I_{de}, I_{dc} are the diffusion capacitance current components.

$$\Rightarrow f_1 \equiv I_{be_{n+1}} + Q'_{je_{n+1}} + \tau_{be} I'_{be_{n+1}} - \alpha_r I_{bc_{n+1}} - I_{b_{n+1}} + I_{bc_{n+1}} + I_{cp_{n+1}}$$
$$+ Q'_{jc_{n+1}} + \tau_{bc} I'_{bc_{n+1}} - \alpha_f I_{be_{n+1}} = 0 \qquad (2.56)$$

The Gear-Shichman approximation is given by

$$X'_{n+1} = \frac{3}{2h} X_{n+1} - \frac{2}{h} X_n + \frac{1}{2h} X_{n-1} \qquad (2.57)$$

where $n+1$ denotes the value of X at $n+1$ time instant, h is the time step, and X' denotes derivative of X with respect to time. All the derivatives of eqn. (2.56) can be approximated using eqn. (2.57) technique and formulae given by eqns. (2.52) to (2.54). The final nodal equation thus obtained is given ahead.

$$f_1 \equiv I_{be_{n+1}}\left(\frac{3\,\tau_{be}}{2\,h}+1-\alpha_f\right)+I_{bc_{n+1}}\left(\frac{3\,\tau_{bc}}{2\,h}+1-\alpha_r\right)-\frac{2\,\tau_{be}}{h}\,I_{be_n}$$
$$+\frac{\tau_{be}}{2\,h}\,I_{be_{n-1}}-\frac{2\,\tau_{bc}}{h}\,I_{bc_n}+\frac{\tau_{bc}}{2\,h}\,I_{bc_{n-1}}-I_{b_{n+1}}+I_{cp_{n+1}}$$
$$+\frac{3}{2\,h}\,Q_{je_{n+1}}-\frac{2}{h}\,Q_{je_n}+\frac{1}{2\,h}\,Q_{je_{n-1}}+\frac{3}{2\,h}\,Q_{jc_{n+1}}$$
$$-\frac{2}{h}\,Q_{jc_n}+\frac{1}{2\,h}\,Q_{jc_{n-1}}=0 \qquad (2.58)$$

Similarly at Node i

$$f_2 \equiv \alpha_f\,I_{bc_{n+1}}-I_{bc_{n+1}}\left(\frac{3\,\tau_{bc}}{2\,h}+1\right)+\frac{2\,\tau_{bc}}{h}\,I_{bc_n}-\frac{\tau_{bc}}{2\,h}\,I_{bc_{n-1}}-\frac{3}{2\,h}\,Q_{jc_{n+1}}$$
$$+\frac{2}{h}\,Q_{jc_n}-\frac{1}{2\,h}\,Q_{jc_{n-1}}-I_{cp_{n+1}}-i_{c_{n+1}}=0 \qquad (2.59)$$

Node c

$$f_3 \equiv i_{c_{n+1}}-I_L+\frac{3\,C}{2\,h}\,v_{c_{n+1}}-\frac{2\,C}{h}\,v_{c_n}+\frac{C}{2\,h}\,v_{c_{n-1}}=0 \qquad (2.60)$$

BCE:

$$f_4 \equiv V_{bb}-v_{b_{n+1}}-I_{b_{n+1}}\,R_{bb}=0 \qquad (2.61)$$

$$f_5 \equiv v_{c_{n+1}}-v_{i_{n+1}}-i_{c_{n+1}}\,R_{cc}=0 \qquad (2.62)$$

$$f_6 \equiv V_{cc}-v_{c_{n+1}}-I_L\,R_L=0 \qquad (2.63)$$

$$f_7 \equiv v_{c_{n+1}}-\frac{2\,h}{3\,C}\,I_{cc}-\frac{4}{3}\,v_{c_n}+\frac{1}{3}\,v_{c_{n-1}}=0 \qquad (2.64)$$

The above equations (f_1 to f_7) represent the complete set of equations required to achieve the transient solution of the PBJT circuit. The Jacobian can be worked

out, and function values can be calculated around the initial guess provided by the DC analysis. For the DC analysis the capacitor will be open circuited and load resistance value can be added to R_{cc}. The procedure for solving the equations remains same, i.e., involving Newton-Raphson iteration method as explained earlier. At each time step solution is thus obtained for transient response.

2.2.2 Inductive Load

The equation set can similarly be generated for the inductive load. In this case load is not purely inductive, but a resistive load is connected in series with inductor for proper biasing of the transistor as shown in Fig. 2.7.

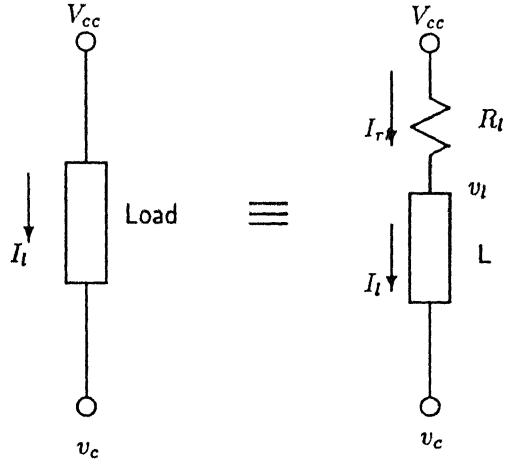

Figure 2.7: Inductive Load Circuit

The changes will be in the function values of f_3, f_6 and due to the addition of node v_l two more functions will be evaluated corresponding to unknowns v_l, I_{rl}. These function values can be obtained with the help of the following equation.

$$I_{L_{n+1}} = \frac{2\,h}{3\,L}\,(V_{cc} - v_{c_{n+1}}) + \frac{4}{3}\,I_{L_n} - \frac{1}{3}\,I_{L_{n-1}} \tag{2.65}$$

This value of $I_{L_{n+1}}$ will replace I_L in the equations of f_3, f_6 to give the set of

equations for transient response with inductive load. During DC analysis inductor will be short circuited. The final set of equations is as given below.

$$f_3 \equiv i_{c_{n+1}} + \left(\frac{3\,C}{2\,h}\right) v_{c_{n+1}} - \left(\frac{2\,C}{h}\right) v_{c_n} + \left(\frac{C}{2\,h}\right) v_{c_{n-1}} - \left(\frac{2\,h}{3\,L}\right) \left(v_{l_{n+1}} - v_{c_{n+1}}\right) - \left(\frac{4}{3}\right) I_{l_n} + \left(\frac{1}{3}\right) I_{l_{n-1}} = 0 \tag{2.66}$$

$$f_6 \equiv v_{l_{n+1}} - v_{c_{n+1}} - \left(\frac{3\,L}{2\,h}\right) I_{l_{n+1}} + \left(\frac{2\,L}{h}\right) I_{l_n} - \left(\frac{l}{2\,h}\right) I_{l_{n-1}} = 0 \tag{2.67}$$

$$f_8 \equiv I_{rl} - \left(\frac{2\,h}{3\,L}\right) \left(v_{l_{n+1}} - v_{c_{n+1}}\right) - \left(\frac{4}{3}\right) I_{l_n} + \left(\frac{1}{3}\right) I_{l_{n-1}} = 0 \tag{2.68}$$

$$f_9 \equiv V_{cc} - v_{l_{n+1}} - I_{rl}\,R_l = 0 \tag{2.69}$$

The remaining function equations i.e., f_1, f_2, f_4, f_5, f_7 remain same. Remaining procedure is identical with the resistive load case. In this way the transient analysis can be performed for PBJT for various types of loads.

Chapter 3

RESULTS AND COMPARISON

The model of PBJT described in the last chapter was implemented with a C-program. The various model parameters include the standard low power transistor model parameters and five additional parameters viz. W, A, τ, N_d, and R_{co}. All the above parameters are already described in detail in the last chapter. The values of the various parameters were obtained from [1],[2]. Using all these values the results for static and dynamic behavior were derived by running model program.

The model parameter values are listed in Table 3.1. For parameters not given in [1],[2] some reasonable values were chosen.

Table 3.1: Device Parameters for Static and Dynamic Analysis

DEVICE PARAMETERS Temp = 24^0C															
h_{FEO}	α_f	α_r	N_d 10^{14} cm^{-3}	W μm	D cm^2/s	A cm^2	τ μs	μ_n $cm^2/Vsec$	I_s pA	C_{jo} nF	τ_{be} μs	τ_{bc} μs	R_{co} Ω	b	V_{bi} V
16.5	0.94	0.5	1.16	50	22.3	0.174	15	1300	2.0	0.46	0.01	3.0	2.69	3	0.8

Note that D is the ambipolar diffusion constant and τ is the miniority carrier lifetime in the lightly doped collector layer.

3.1 DC Characteristics

The DC characteristics were obtained for the model PBJT as mentioned earlier (given in Fig. 2.2). These curves along with the results from [1],[2] are given in Fig. 3.1 and Fig. 3.2. The curves are obtained for different base drives as indicated in the graphs.

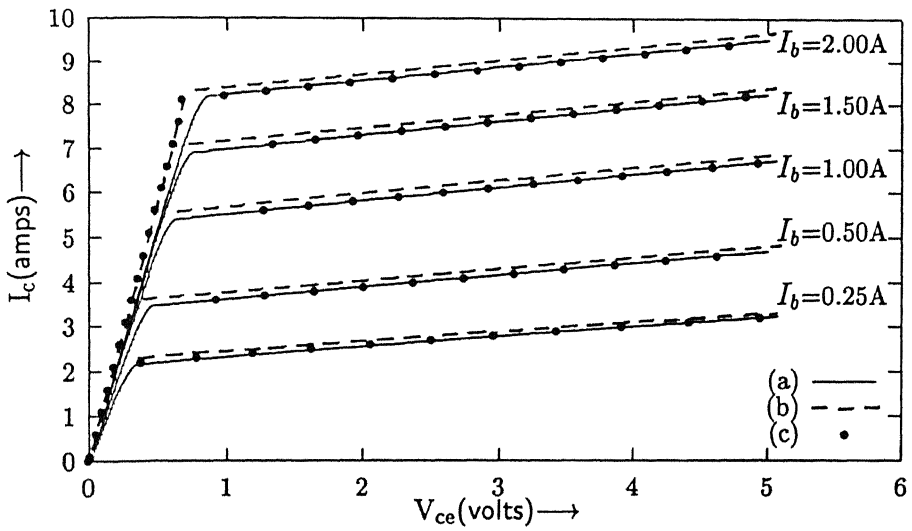

Figure 3.1: PBJT DC Characteristics for Higher Value of I_b (a) Model Results (b) Results of [1] (c) Results of [2]

The curves of [1] do not take into account the collector lifetime τ, whereas effects of τ have been accounted for in [2]. The model results are in good agreement with results of [2], which further shows the validity of the model. There are two distinct regions in the characteristics of Fig 3.1 and three regions in Fig. 3.2. The first slope indicates hard-saturation region, the second slope indicates quasi-saturation region, and the final one being active region.

In the quasi-saturation regime, the behavior of the PBJT is basically dominated by the charge stored in the collector layer. Also the collector layer lifetime is very important in determining the PBJT behavior because recombination current I_{cp}

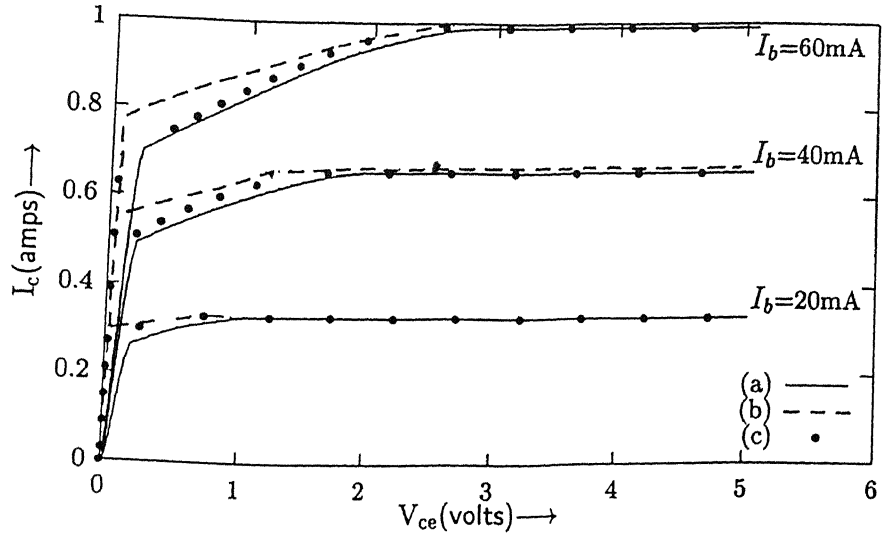

Figure 3.2: PBJT DC Characteristics for Lower Value of I_b (a) Model Results (b) Results of [1] (c) Results of [2]

is affected by this lifetime. All these factors are taken into consideration in the derivation of this model.

3.2 Transient Behavior

3.2.1 Resistive Load

The transient characteristics are also obtained by using the procedure mentioned in the last chapter. The various model parameters and the component values are taken from [1],[2] for comparison of results. The PBJT is switched on and off by applying a base drive of $+2$ V and -2 V respectively. The change in the base drive voltage is assumed to be instantaneous, i.e., from 0 to $+2$ V for turning on and from $+2$ V to -2 V for turning off. The PBJT is off at time $t = 0^-$ and turn on is initiated at time $t = 0$. Figures. 3.3, 3.4, and 3.5 give the various current and voltage waveforms obtained by simulation of the circuit shown in Fig. 2.4. Here

base drive changes polarity at t = 20 μsec during turn off. The arrow in the time axis indicates the time at which turn off is initiated.

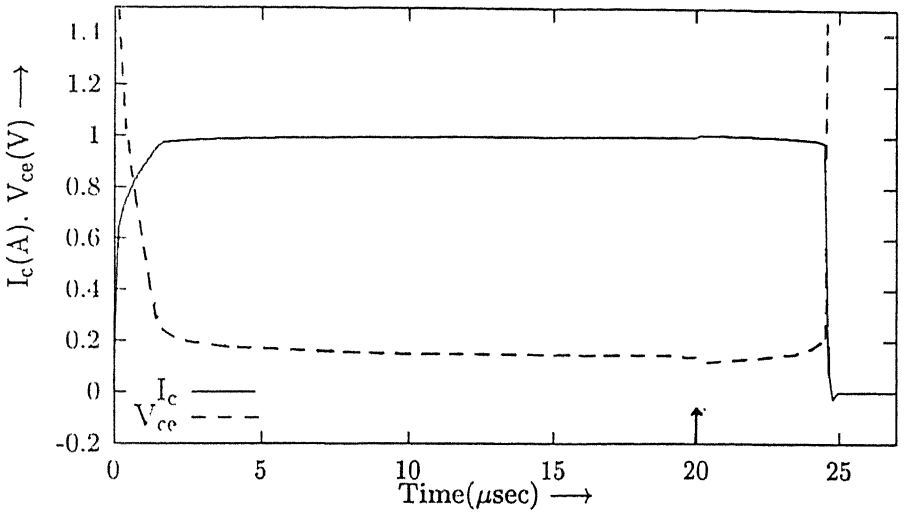

Figure 3.3: Transient Current/Voltage Waveforms for $R_l = 3.6\ \Omega$ (I_c, V_{ce})

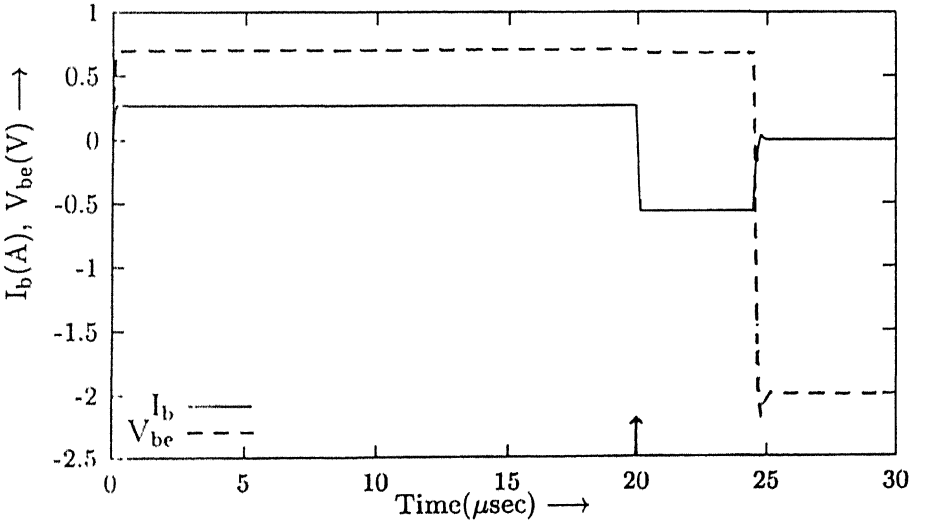

Figure 3.4: Transient Current/Voltage Waveforms for $R_l = 3.6\ \Omega$ (I_b, V_{be})

All the waveforms are obtained for the purely resistive load of 3.6 Ω, V_{cc} of 3.7 V

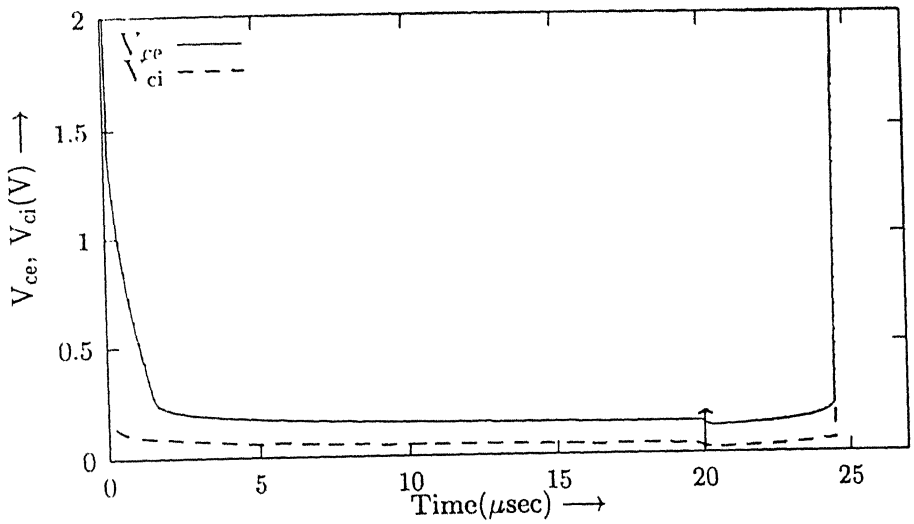

Figure 3.5: Transient Voltage Waveforms for $R_l = 3.6\ \Omega$ (V_{ce}, V_{ci})

and snubber capacitor of 1 nF. The base biasing resistor is of 5 ohms. A saturation resistance of 0.085 ohms is assumed for plotting V_{ce} waveform. Figure 3.5 shows the comparison between the internal and external collector voltage. The time step of $\tau/100$ is taken for simulation of current/voltage transients. The error margin was fixed at 10^{-5} for calculation of all the currents and voltages. The effects of changing the error margin, base drive, and time step are dealt in detail later in the chapter.

We now compare the waveforms of Fig. 3.3 with the experimental results taken from [1]. Figure 3.6 gives the results for the turning on of PBJT. In [1], the turning on process was modelled assuming two distinct time constants. The model results are in quite good agreement with results of [1]. Both the curves are obtained for load resistance value of 3.6 Ω. The comparison curves validate the model results for the turning on process.

In [1] the turn on transients were given for another value of load resistance as well. The simulated results are also worked out for this case where the load resistance is of 20.8 Ω and V_{cc} of 21 V. In Fig. 3.7, the comparison between the

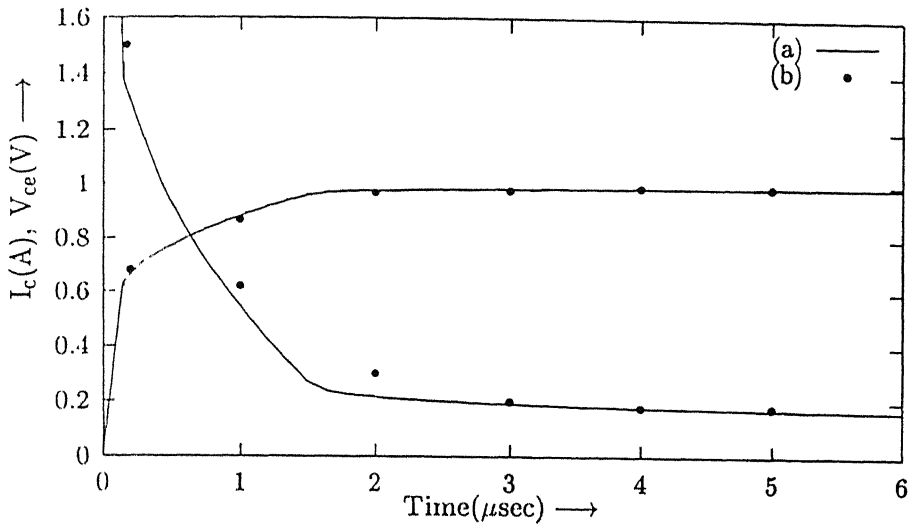

Figure 3.6: Comparison Curves with $R_l = 3.6\ \Omega$ (a) Simulated (b) Results from [1]

simulated and experimental data is given.

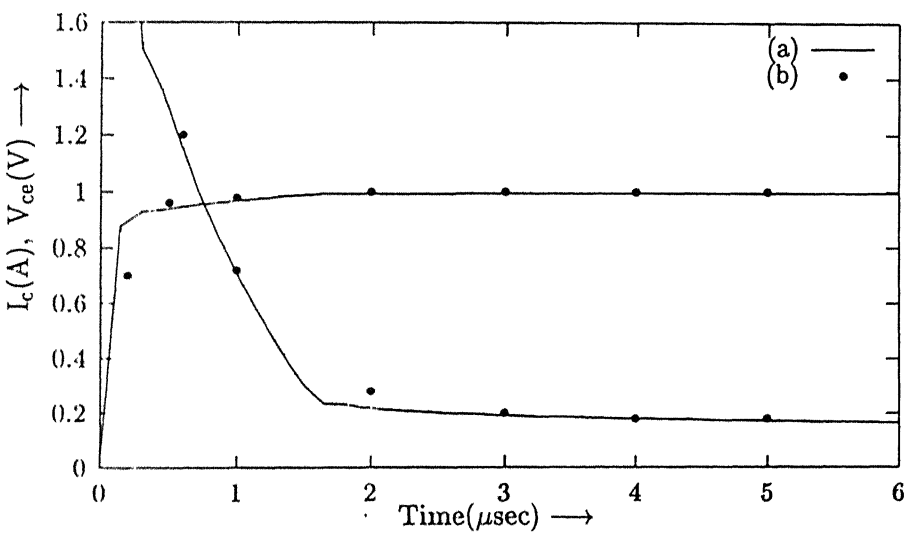

Figure 3.7: Comparison Curves with $R_l = 20.8\ \Omega$ (a) Simulated (b) Results from [1]

Here also there is good agreement between the simulated and experimental re-

sults. This further validates the model. All waveforms for a resistive load of 20.8 ohms are given in Figs. 3.8 to 3.10.

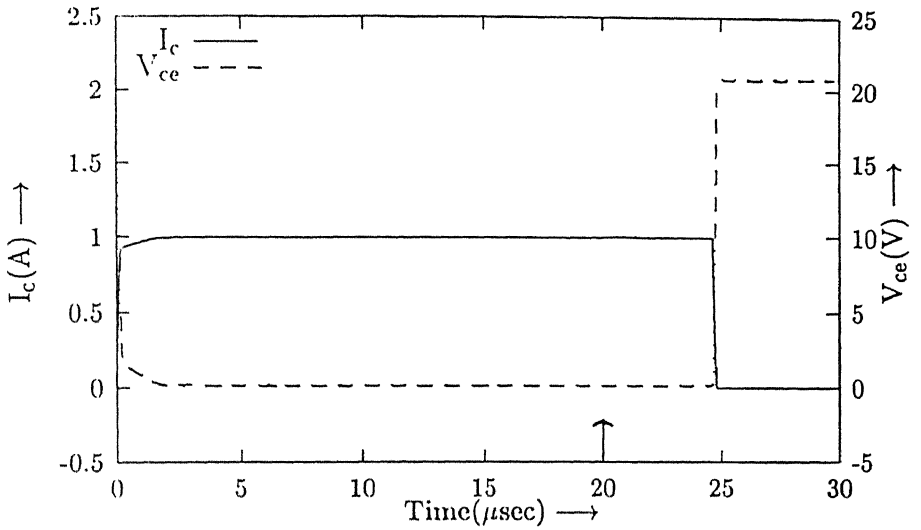

Figure 3.8: Transient Current/Voltage Waveforms for $R_l = 20.8\ \Omega$ (I_c, V_{ce})

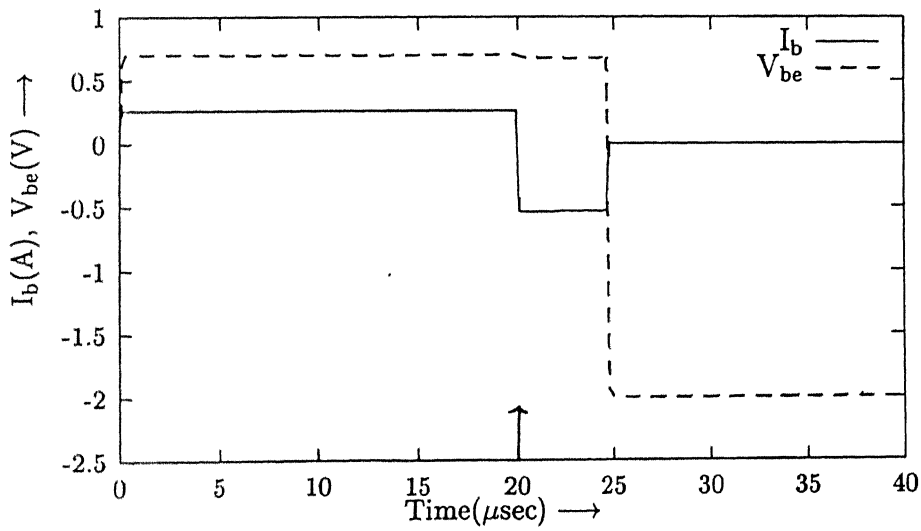

Figure 3.9: Transient Current/Voltage Waveforms for $R_l = 20.8\ \Omega$ (I_b, V_{be})

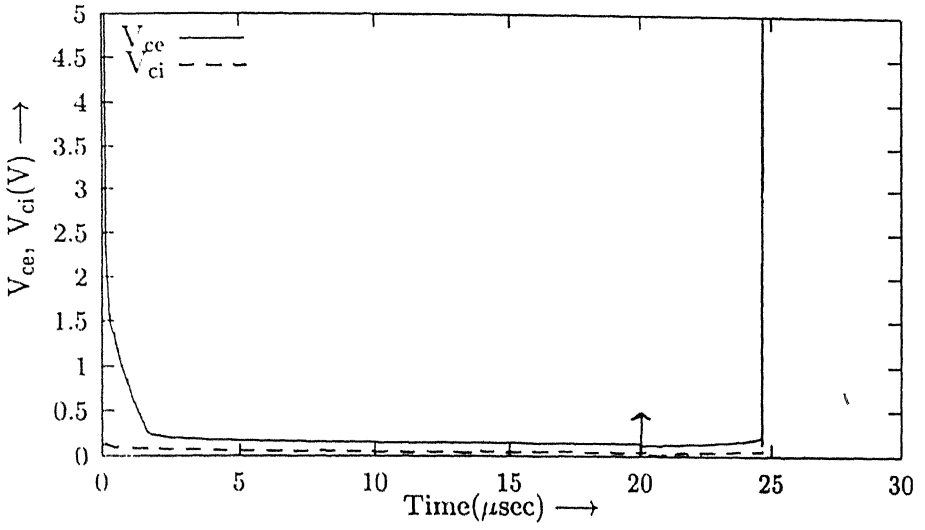

Figure 3.10: Transient Voltage Waveforms for $R_l = 20.8\ \Omega$ (V_{ce}, V_{ci})

The turn off results cannot be validated due to the non-availability of the experimental data for the model transistor. However, a good qualitative agreement is achieved by comparison of the shape of the various waveforms with the usual shape of turning of results of PBJT as given in [7]. The model was tested under various bias conditions with different combinations of supply voltage and loads. During the various simulations it was noted that a proper selection of bias point is crucial.

3.2.2 Inductive Load

The model transistor's transient characteristics were also checked with inductive load (Fig. 2.4 and 2.7). All the model parameters remain same except the snubber capacitor in this case was taken to be 10 nF. A resistive load of 24 Ω was connected in series with the inductive load for proper biasing of transistor. The supply voltage V_{cc} was kept at 25 V. The same base drive was used to switch the transistor on and off. Again switching off was initiated at time t = 25 μsec. The time step and the error margin setting remains same as in resistive load case. Figures 3.11 to 3.14 give the various current and voltage waveforms for an inductive load of 10 μH.

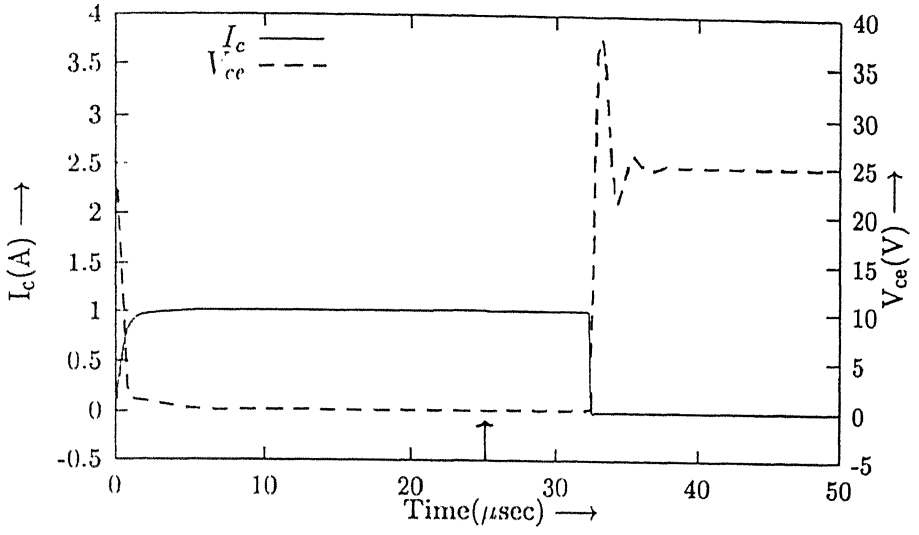

Figure 3.11: Transient Current/Voltage Waveforms for Inductive Load (I_c, V_{ce})

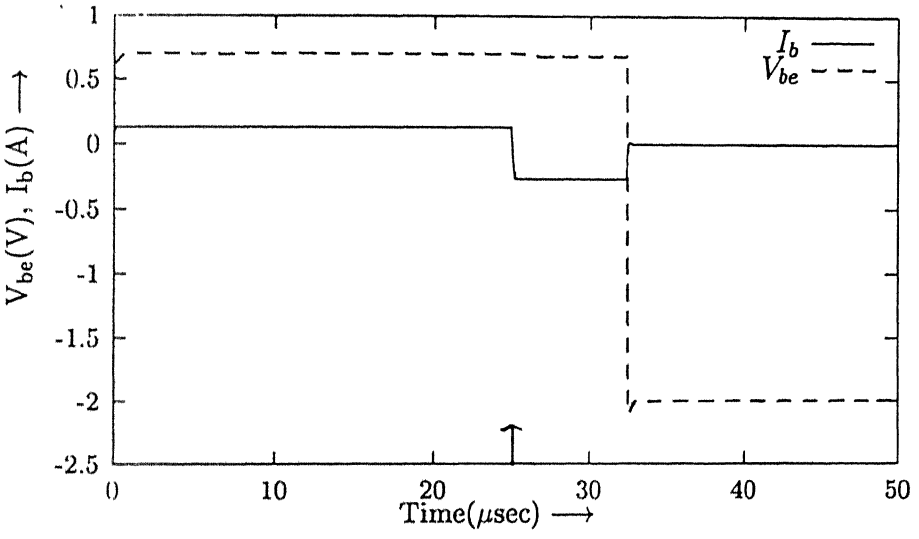

Figure 3.12: Transient Current/Voltage Waveforms for Inductive Load (I_b, V_{be})

The period of the oscillations during the turning off of PBJT in Fig. 3.11 is a function of L and C. In practical cases, as the capacitor will be replaced by diode, oscillations will not occur. Also it is quite evident that turning on/off takes longer time with the addition of inductive load as compared with purely resistive load.

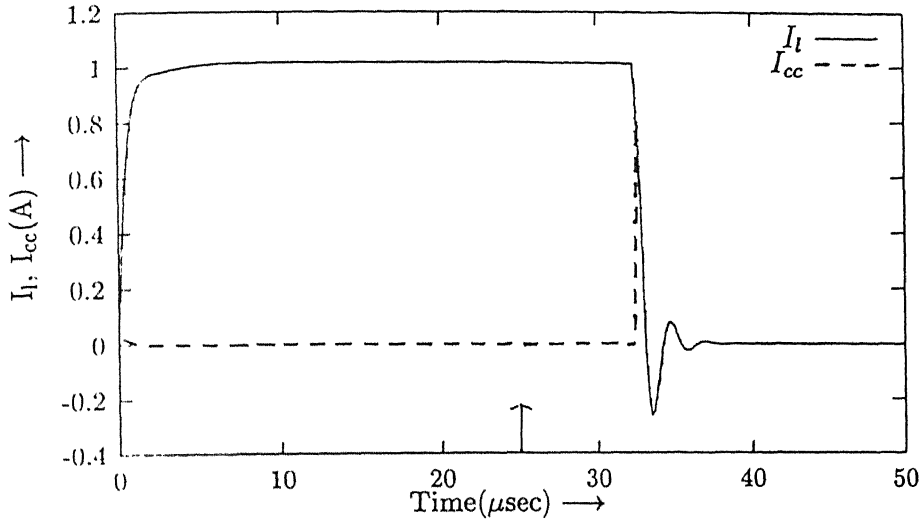

Figure 3.13: Transient Current Waveforms for Inductive Load (I_l, I_{cc})

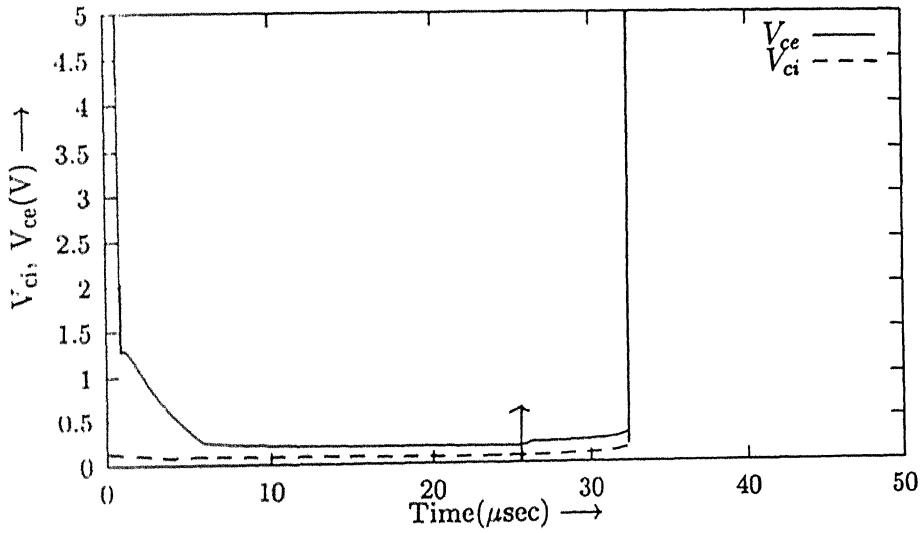

Figure 3.14: Transient Voltage Waveforms for Inductive Load (V_{ce}, V_{ci})

The waveforms of current through inductor and capacitor (I_l, I_{cc}) are given in Fig. 3.13. During the turning on I_l follows I_c and $I_{cc} = 0$, i.e. no current flows through the snubber capacitor. During turning off when I_c goes to zero, all the current goes through the capacitor. This is very clear from Fig. 3.13. Basically

the KCL at the node c is always maintained, i.e., $I_L = I_c + I_{cc}$.

The comparison between the internal and external collector voltage (V_{ce}, V_{ci}) is given in Fig. 3.14. The difference in the voltages is due to the voltage dropped in the drift region, i.e., across the resistance R_{cc} in the model.

As there is no experimental data available in literature for transient behavior with inductive load, we could not validate the model quantitatively in this case. However, the qualitative agreement exists by comparing the shape of waveforms with [7].

3.3 Effect of Varying Base Drive

The transient behavior of the device depends significantly on the base drive. A high base current reduces the switching losses for turn on but will increase the switching off time and losses for the turning off. This is due to the fact that though higher base current will switch on the PBJT faster, during turn off the storage time as depicted by base current waveform will increase resulting in higher switching off time. Reverse base drive will also determine the switching off time. The PBJT can be turned off by making base supply voltage zero or negative. The turn off time is basically function of the charge stored in the drift region because that much charge is to be removed to turn off the transistor. The stronger the negative base drive less time will be taken for transistor to turn off.

The above effects were verified with the model developed. The model transistor was switched on by V_{bb} going instantaneously from 0 to 2 V and in another case from 0 to 4 V at time t=0. The reverse base drive was kept same for both the cases i.e. at -2 V. All the remaining parameters and component values were also kept constant. Figures 3.15 to 3.19 give the various comparison curves for the above mentioned two cases.

Figure 3.15 gives the expanded view of the turning on process. Clearly by taking

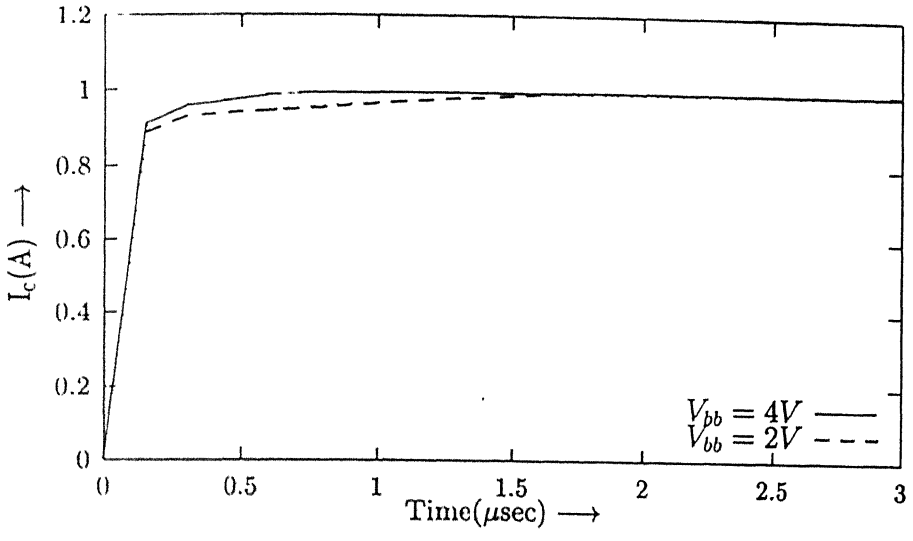

Figure 3.15: Effect of Different Base Drives on I_c during turn on (Expanded View)

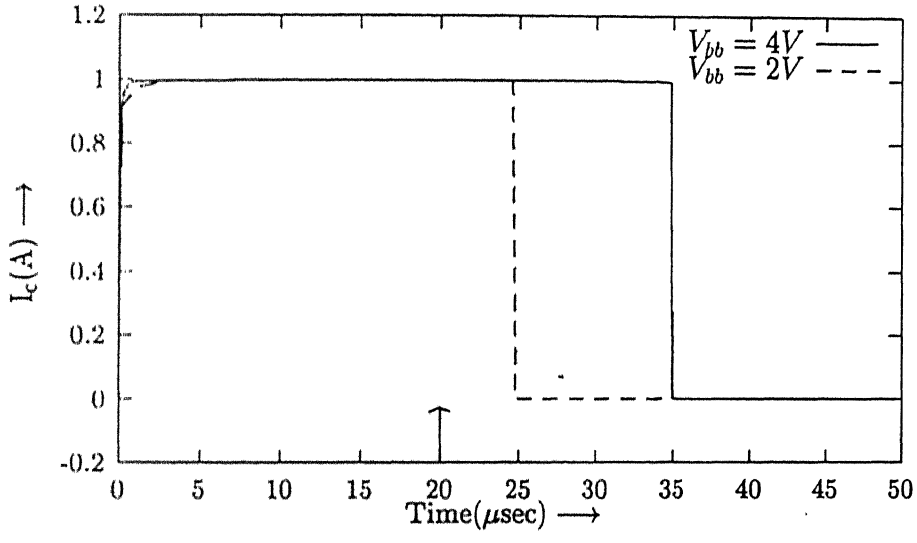

Figure 3.16: Effect of Different Base Drives on I_c during turn on

a strong base drive the process of turning on has become faster. The 4 V V_{bb} drive makes the transistor reach the 90 percent of I_c value faster than 2 V base drive. The effect of this decrease in turning on time on the turning off time can be seen in Figs. 3.16 to 3.19. All of these waveforms correspond to the resistive load value

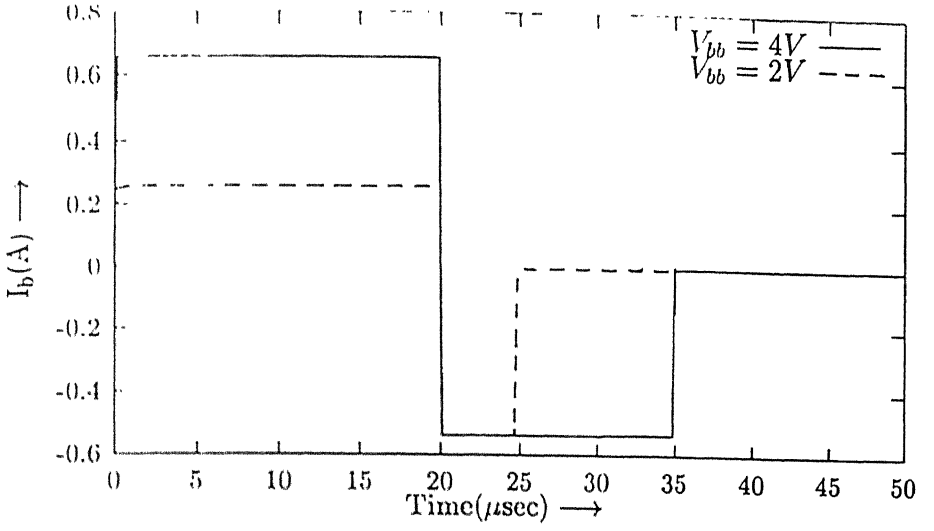

Figure 3.17: Effect of Different Base Drives on I_b during turn on

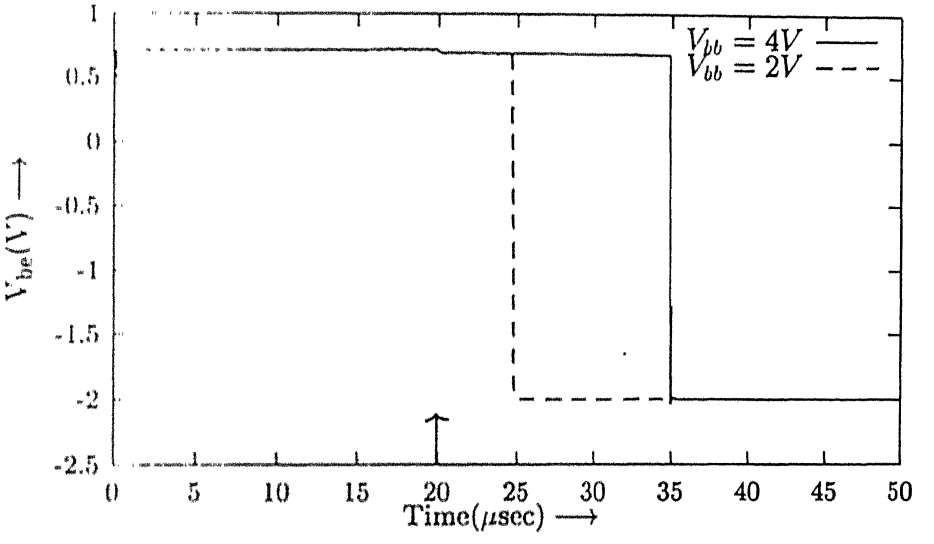

Figure 3.18: Effect of Different Base Drives on V_{be} during turn on

of 20.8 ohms. Also the time step is set at $\tau/100$ and error margin at 10^{-5}.

From all the above waveforms it is clear that, a stronger forward base drive improves turn on but degrades turn off performance. Thus the choice of base drive

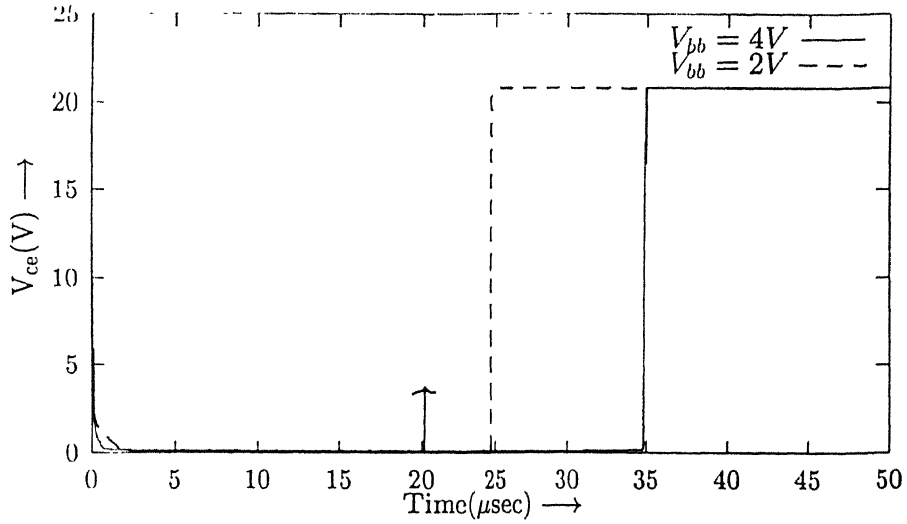

Figure 3.19: Effect of Different Base Drives on V_{ce} during turn on

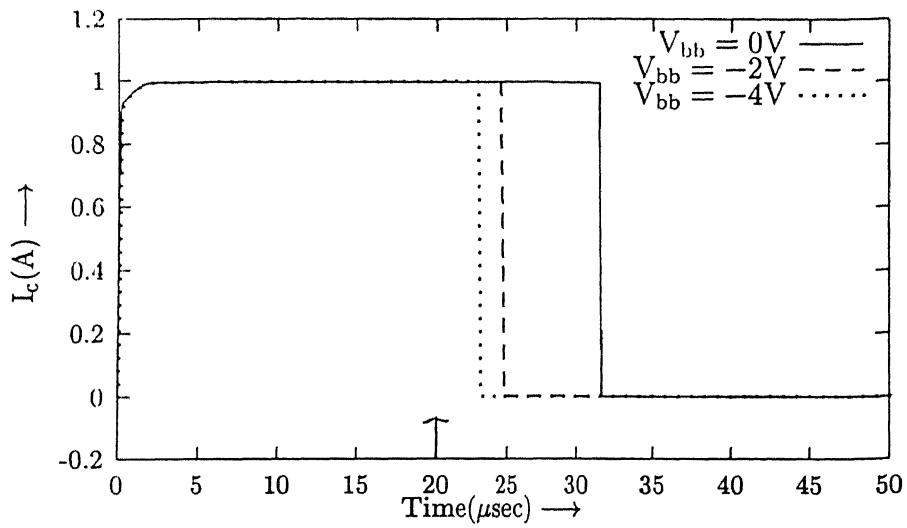

Figure 3.20: Effect of Different Base Drives on I_c during turn off

for turning on of PBJT is very critical. In the following analysis it is shown that how the turning off base drive affects the dynamic behavior of PBJT.

The model transistor was switched off with three different base supply voltages,

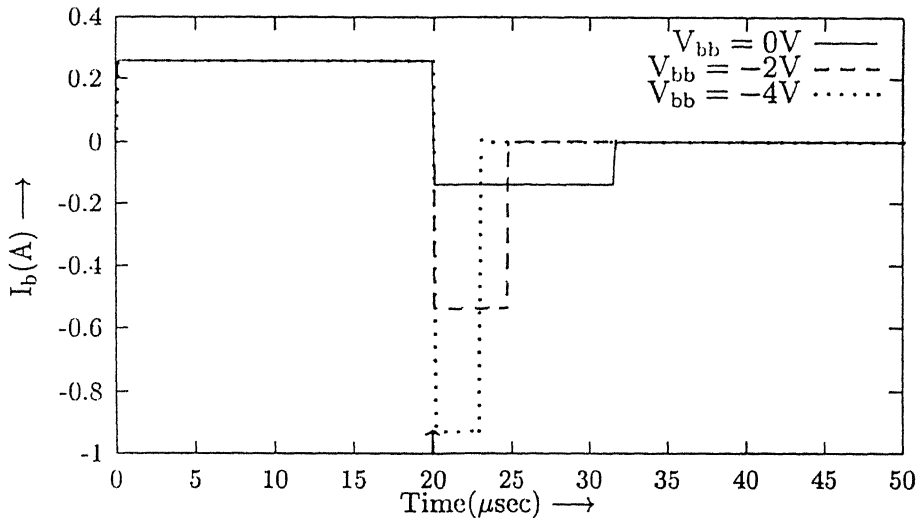

Figure 3.21: Effect of Different Base Drives on I_b during turn off

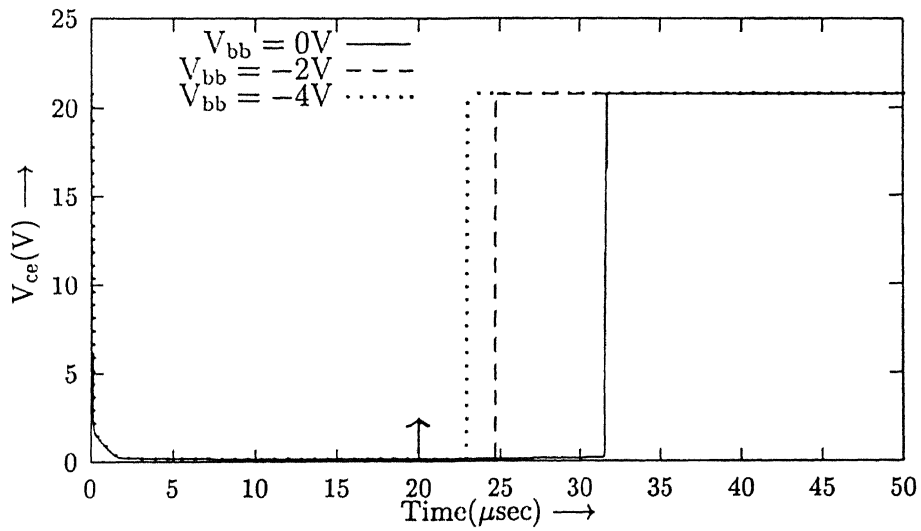

Figure 3.22: Effect of Different Base Drives on V_{ce} during turn off

i.e., 0 V, -2 V, -4 V. In all the three cases the transistor was switched on with same base drive, i.e., 2 V of V_{bb}. All the remaining parameters were kept same. Figures 3.20 to 3.23 give the various current/voltage waveforms under different bias conditions.

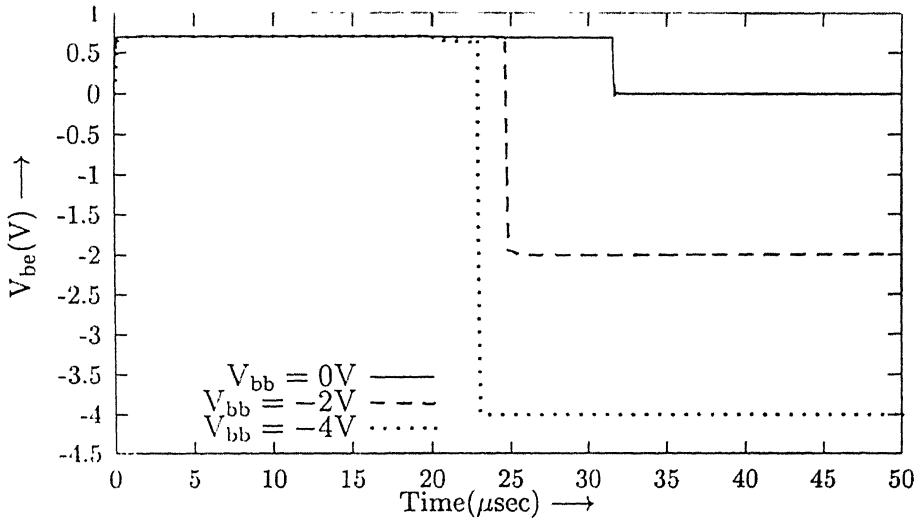

Figure 3.23: Effect of Different Base Drives on V_{be} during turn off

It is evident from these figures that as we keep on increasing the reverse base drive the switching off time decreases. This is to be expected as a large reverse bias removes the excess charge faster.

3.4 Effect of Changing Time-Step

The choice of the time step is very crucial for transient analysis. If the time step is too large then the transient behavior of a device can be missed out and on the other hand if time step is too small then the number of time instants for which calculation of currents/voltages is required will be too many, resulting in increase in simulation time. Thus there is a need to select optimum time step.

The transient behavior of PBJT is governed mainly by the charge in the drift region. This charge is a function of collector drift region lifetime τ. Thus if time-step is chosen less than the value of τ the transient behavior can be modelled properly. On repeated simulations it was found that the value of time step of $\tau/100$ is quite reasonable for PBJT transient analysis. The effect of varying the

time step on the transient behavior is given in Figures 3.24 to 3.27.

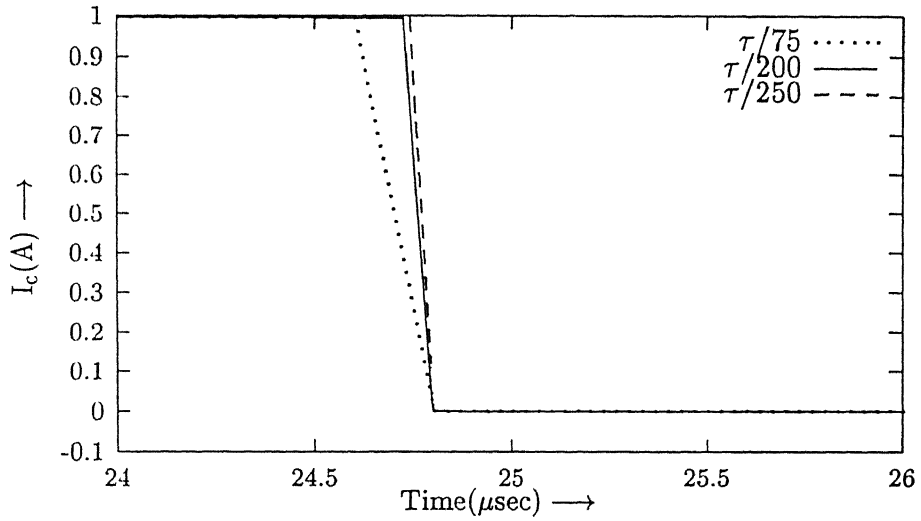

Figure 3.24: Effect of Change in Time Step on I_c

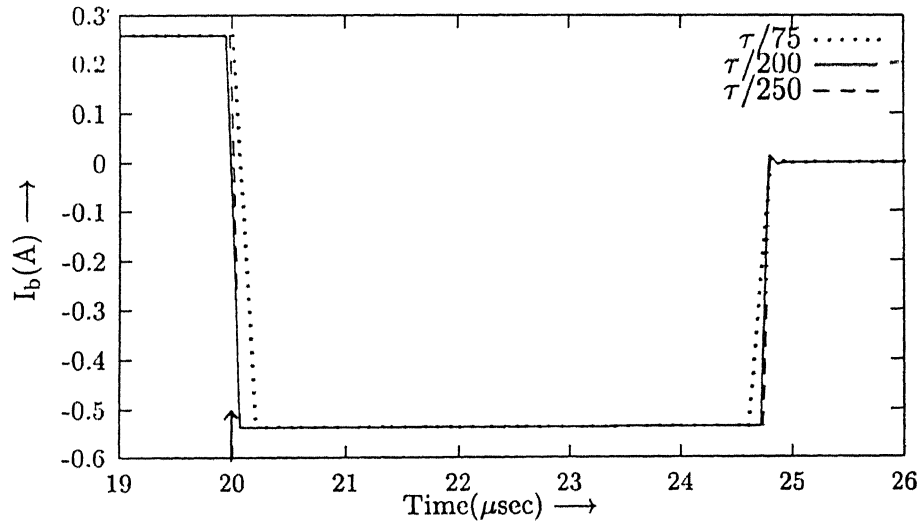

Figure 3.25: Effect of Change in Time Step on I_b

The turn on transients were relatively unaffected by time step. Hence, only the turn off transients for various currents/voltages are given in previous figures. It is

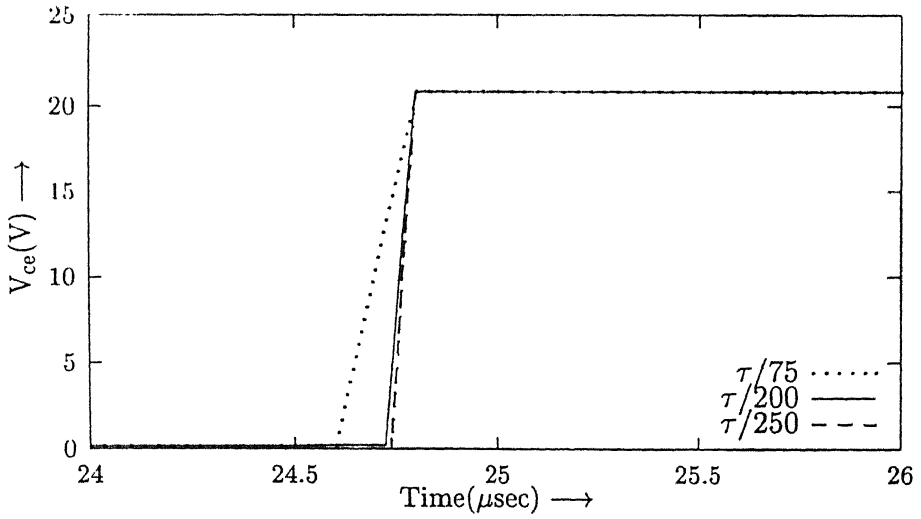

Figure 3.26: Effect of Change in Time Step on V_{ce}

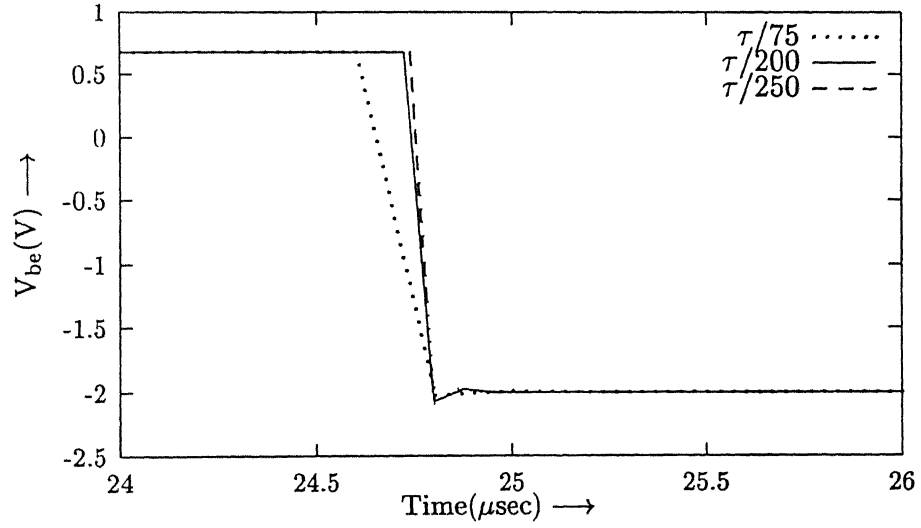

Figure 3.27: Effect of Change in Time Step on V_{be}

interesting to see that beyond a certain time step, i.e., $\tau/200$ the solution does not change significantly. Thus time step smaller than this will only waste CPU time.

3.5 Effect of Changing Error Margin

The selection of error margin is very important in circuit simulation. This is because the equation solving procedure is iterative in nature. The procedure is said to have converged if the variables differ from the previous iteration by less than the specified error margin. Thus convergence is a function of acceptable error margin. A high value of error margin will lead to faulty results and on the other hand a very low value will lead to a lot many iterations where sometimes oscillations can occur giving no result at all. Therefore, there is need to select optimum error margin such that number of iterations are less and the results are reasonably accurate.

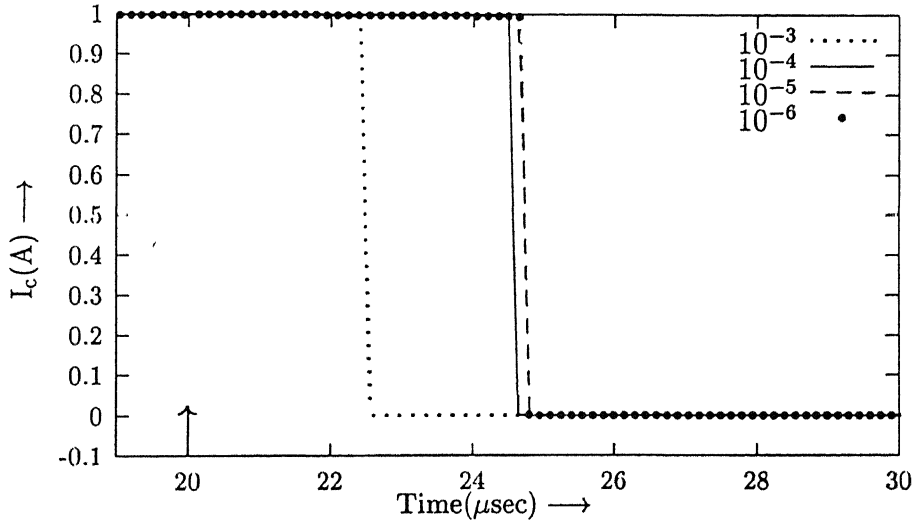

Figure 3.28: Effect of changing Error Margin on I_c

In the present model development the effect of changing error margin was studied to select the optimum value. Keeping the various model parameters, component values and supply voltages constant, the error margin was varied from 10^{-3} to 10^{-6}. This range of error margin was selected because various currents/voltages in PBJT are much higher than this range, i.e., error possible with 1 amp/volt will be in mA/mV respectively. The waveforms of various currents/voltages thus obtained are given in Figs. 3.28 to 3.31. From the waveforms it is evident that beyond the

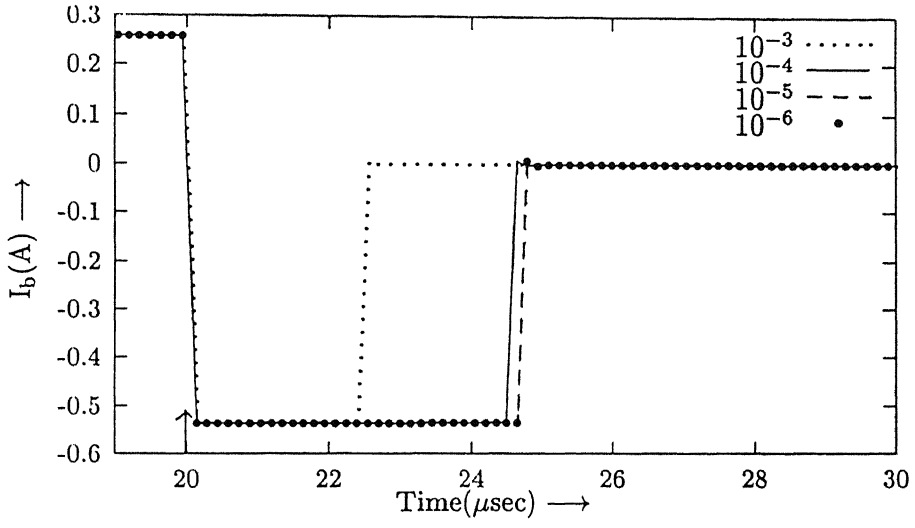

Figure 3.29: Effect of changing Error Margin on I_b

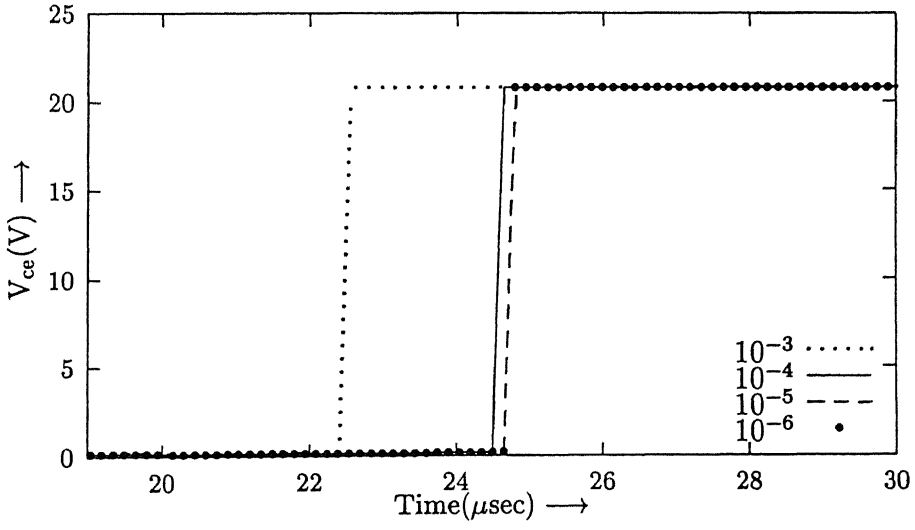

Figure 3.30: Effect of changing Error Margin on V_{ce}

error margin of 10^{-5} , the solution does not change noticeably. Thus the error margin value of 10^{-5} is most suitable for the present circuit simulation.

All the waveforms presented are for turn off transients only as the results in

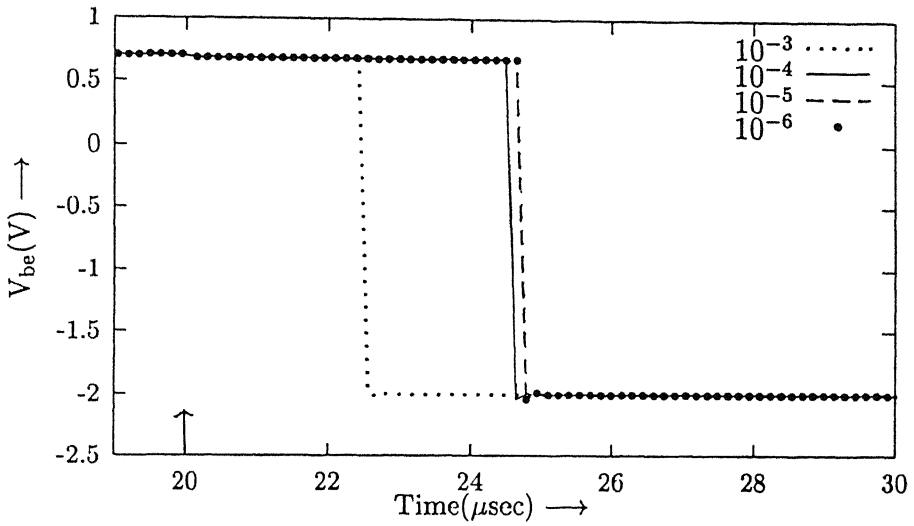

Figure 3.31: Effect of changing Error Margin on V_{be}

the turning on transients did not show significant changes for the selected range of error margin. Also it is interesting to note that there is a remarkable shift in solution when we change from error margin of 10^{-3} to 10^{-4} whereas further change in error margin results in very small shift in the solution and finally solution does not change appreciably beyond an error margin of 10^{-5}. This was the reason for selecting this value for PBJT simulation under different bias conditions.

3.6 Charge Profile During Turn on/off

The dominant difference between a PBJT and a low voltage transistor arises due to the stored charge in the drift region. During the turn on process the charge keeps on building up till it reaches its steady state value as decided by the bias conditions and during turn off process the stored charge gets removed as per the reverse base drive condition. We have already seen how the time for removal/storage of charge varies with the t bias conditions. However, it is very interesting to actually capture the charge profile at different time instants during turning on/off.

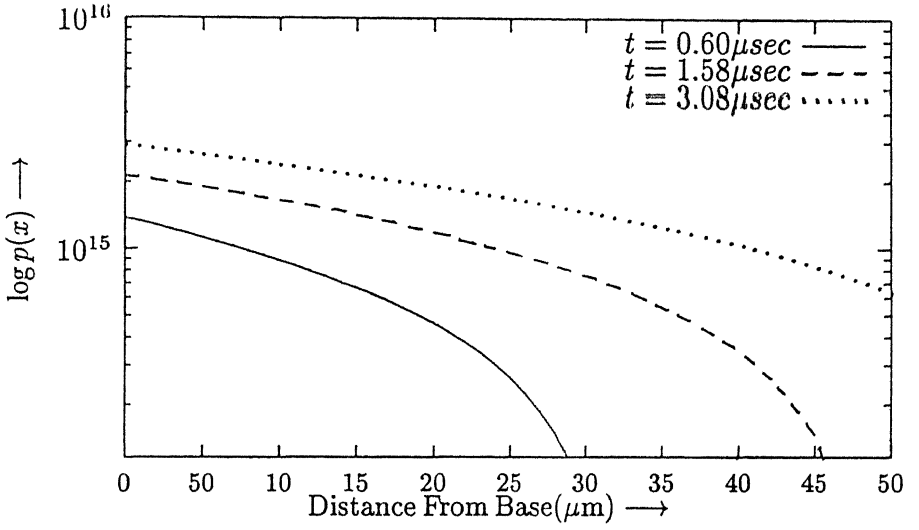

Figure 3.32: Charge Profile in Drift Region of PBJT during turn on

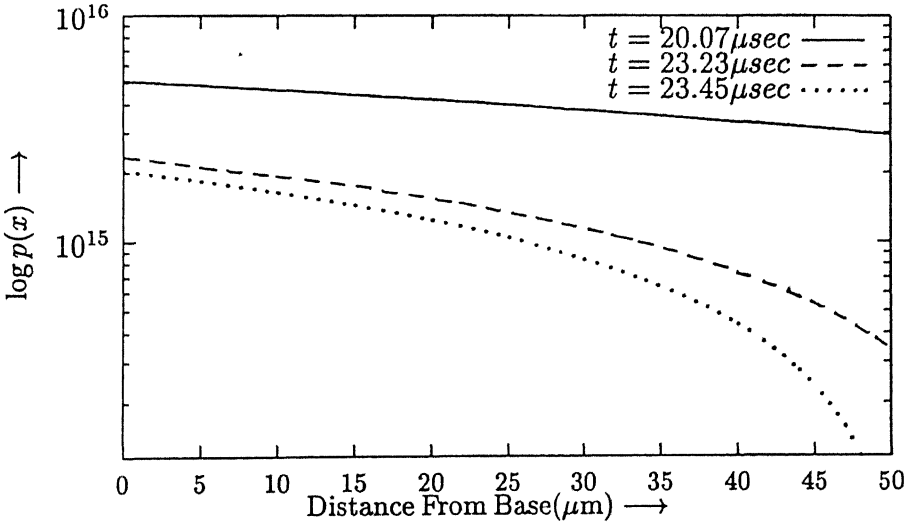

Figure 3.33: Charge Profile in Drift Region of PBJT during turn off

The charge profile in the collector drift region was captured during turning on/off at the various time instants. These are shown in Figs. 3.32 and 3.33. All the curves correspond to the load of 20.8 Ω and remaining parameter values same as before.

From both the figures it is very clear how the PBJT charge builds up during turning on and how it discharges during turning off. During removal of charge after the time instant 23.5 μsec the depletion region forms at collector base junction and charge profile changes to bisinusoidal function. This profile is there for very small time, therefore it was not captured.These two figures helps in actually understanding the buildup and removal of charge in the drift region of PBJT.

Chapter 4

CONCLUSIONS AND FUTURE WORK

The present model has been developed taking into account the recombination current and voltage drop in the lightly doped drift region. In the development of this model, several approximations were made which need to be discussed with respect to its application.

The first approximation is that the device is one dimensional, and none of the two dimensional aspects was considered during model development. This was assumed to keep the governing differential equations simple. However, practically this assumption is valid only if the device is very fine structured, which is normally the tendency for the current development of the power devices. The devices with larger structure have two dimensional effects such as current crowding and these cannot be neglected. These are not incorporated in the present model. One possible solution is to use a parallel connection of several PBJT models as shown in Fig. 4.1 [5].

Here the real transistor is separated into different slices. Now each slice can be described as a single PBJT model. All the collectors and emitters are connected as shown in the figure. Base resistors are inserted between the bases whose resistance

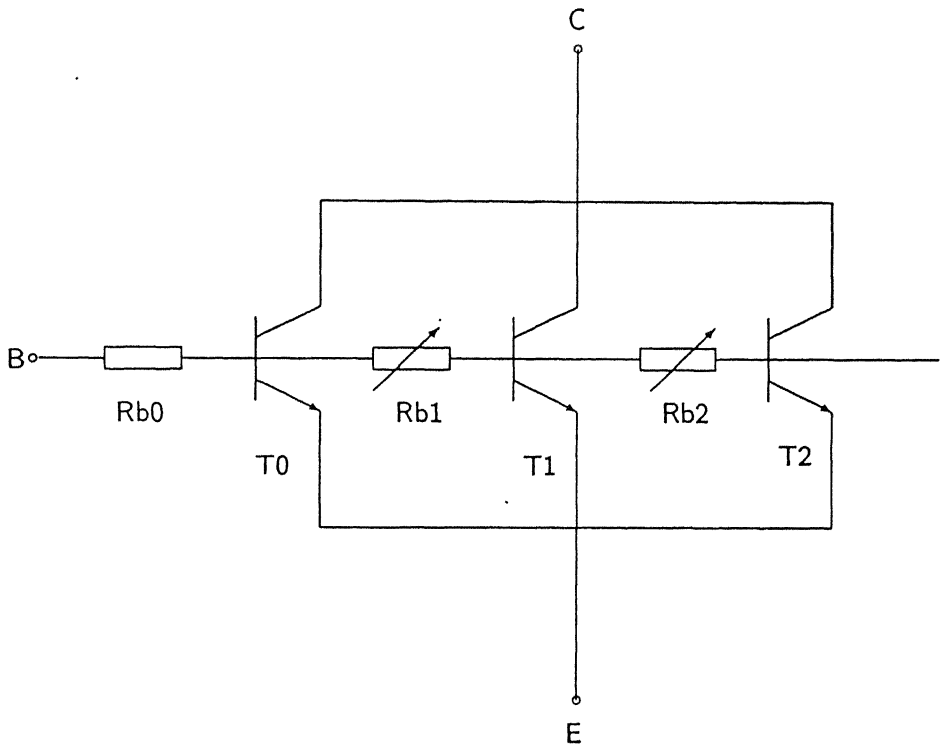

Figure 4.1: Two Dimensional PBJT Model

values are controlled by the injection in base, the base-emitter and base-collector voltages of the two adjacent transistors. In this way 2-D effects in PBJT model can be implemented.

The other important approximation is $\partial p/\partial t = p/T$ for certain regions as discussed in Chapter 2. There are four types of charge profiles possible during turn off. These are hyperbolic, linear, sinusoidal and bisinusoidal. During turning off the charge profile changes from one form to the other at different time instants. The change of its form depends on the bias and the carrier lifetime. The stronger the change, higher is the deviation of the approximation. Thus we can say that the inaccuracy of the model increases with the switching speed. However, in the absence of this approximation p is a function of position as well as time, and eqn. (2.27) cannot be reduced to an ordinary differential equation. Thus to keep sim-

plicity in the model, approximation is made and as discussed in last chapter, results are qualitatively correct.

Besides the stored charge in the collector layer, there are stored charges in the base and emitter as well. The space charges are described as the depletion capacitance. The excess charge in the emitter is negligible due to high doping whereas, the charge in the base has very complex characteristics due to structure, doping and the biases. This is due to the reason that base has no uniform doping and base current is two dimensional, one in the collector emitter direction and one in the cross direction. As the charge in the base is much lower than the charge in the collector drift region, the approximation in the standard model of the diffusion charge can be used. This was done while developing the equivalent circuit of the PBJT to give the transient behavior.

We now briefly discuss parameter extraction which is very important for device simulation. The model contains a standard transistor model and two additional elements (I_{cp}, R_{cc}). Besides the parameter chosen, there are five additional parameters for the two new elements (A, N_d, W, R_{co}, τ). The first four parameters can be estimated from the device processing details. The most important parameter τ can be found out using quasi-saturation analysis as given in [4]. The remaining parameters pertain to the standard transistor model and can be evaluated as given [5]. As the parameter extraction was not the main task in the present work, the detailed extraction procedure is not presented here.

In the present work the PBJT is treated as a normal circuit element, i.e., its equations are solved along with the normal circuit elements like resistors, capacitors etc. [6]. The equation formulation for the PBJT is done by studying the physics of the device [7],[8],[9]. This particular procedure is not only valid for PBJT but can be extended for any low voltage or power device. Also this is the basic procedure adopted in any circuit simulator like SPICE.

This model does not take into account the effect of parameters changing with the operating temperature. Also the second breakdown effect is not included in

the model. These aspects can be exploited further in future work. As such this model provides a good designing tool for power bipolar transistor having $n^+ p \nu n^+$ geometry. Also as a future work this model can be incorporated in SPICE as a separate model for PBJT. This can be done by adding the various equations presented for PBJT in the standard transistor model of SPICE.

REFERENCES

[1] Philip L. Hower, " Application of a Charge-Control Model to High-Voltage Power Transistors," *IEEE Trans. Electron Devices*, vol. ED-23, pp. 863-870, Aug. 1976.

[2] K. N. Bhat, M. Jagadesh Kumar, V. Ramasubramanian, and Peter George, "The Effects of Collector Lifetime on the Characteristics of High-Voltage Power Transistors Operating in the Quasi-Saturation Region," *IEEE Trans. Electron Devices*, vol. ED-34, pp. 1163-1169, May 1987.

[3] R. Widlar, "Turn-Off Processes in High-Voltage $n\,p\,v\,n$ Switches," *IEEE Trans. Electron Devices*, vol ED-34, pp. 2013-2022, Sept. 1987.

[4] M. Jagadesh Kumar and K. N. Bhat, "Collector Recombination Lifetime from the Quasi-Saturation analysis of High Voltage Bipolar Transistors," *IEEE Trans. Electron Devices*, vol. 37 No. 2, pp. 2395-2398, Nov. 1990.

[5] Chihao Xu and Dierk Schröder, "Power Bipolar Junction Transistor Model Describing Static and Dynamic Behavior," *IEEE Trans. Power Electronics*, vol.-7, pp. 734-740, Oct. 1992.

[6] William J. McCulla, "Fundamentals of Computer Aided Circuit Simulation," Kluwer Academic Publishers, Boston, 1988.

[7] Ned Mohan, Tore M. Undeland, and William P. Robins, "Power Electronics: Converters, Applications, and Design," John Wiley and Sons Inc., 1989.

[8] Adolph Blicher, "Field Effect and Bipolar Power Transistor Physics," Academic Press Inc., 1981.

[9] Sorab K. Ghandhi, " Semiconductor Power Devices," John Wiley and Sons Inc., 1977.